

# Modeling the spatially distributed nature of subglacial sediment transport and erosion

Ian Delaney<sup>1</sup>, Leif Anderson<sup>1,2</sup>, and Frédéric Herman<sup>1</sup>

<sup>1</sup>Institut des dynamiques de la surface terrestre (IDYST), Université de Lausanne, Bâtiment Géopolis, CH-1015 Lausanne

<sup>2</sup>Department of Geology and Geophysics, University of Utah, Frederick Albert Sutton Building, 115 S 1460 E, Salt Lake City, UT 84112-0102, USA

**Correspondence:** Ian Delaney (IanArburua.Delaney@unil.ch)

**Abstract.** ~~In Glaciers expel sediment as they melt, in~~ addition to ice and water, ~~glaciers expel sediment.~~ As a result, changing glacier dynamics and melt ~~result in produce~~ changes to glacier erosion and sediment discharge, which can impact the landscape surrounding retreating glaciers, as well as communities and ecosystems downstream. To date, ~~available numerical~~ models that transport subglacial sediment on sub-hourly to decadal scales are ~~in one-dimension one-dimensional~~, usually along a glacier's  
5 flow line. Such models have proven useful in describing the formation of ~~glacial~~ landforms, the impact of sediment transport on glacier dynamics, and the interactions among climate, glacier dynamics, and erosion. However, these models omit the two-dimensional spatial distribution of sediment and its impact on sediment connectivity ~~, i.e.,~~ the movement of sediment between its detachment in source areas and its deposition in sinks. ~~In turn, there is a need for modeling~~ ~~Here, we present a numerical model that fulfills a need for predictive~~ frameworks that describe subglacial sediment discharge in two spatial dimensions ( $x$   
10 and  $y$ ) over time. ~~Here, we present~~ SUGSET\_2D ~~, a numerical model that~~ evolves a two-dimensional subglacial till layer in response to bedrock erosion and changing sediment transport conditions ~~below glaciers.~~ Experiments performed using an idealized alpine glacier illustrate the heterogeneity in sediment transport and bedrock erosion ~~below glaciers. The experiments show an the glacier. An~~ increase in sediment discharge ~~following follows~~ increased glacier melt, as has been documented in field observations and other numerical experiments. We ~~also~~ apply the model to a real alpine glacier. ~~Model outputs are compared with annual observations,~~ ~~Griesgletscher in the Swiss Alps, where we compare outputs with annual measurements of sediment discharge measured from Griesgletscher in the Swiss Alps.~~ SUGSET\_2D ~~reproduces accurately reproduces the~~ general quantities of sediment discharge and the year-to-year sediment discharge pattern measured at the glacier terminus. The model's ability to match the ~~data depends greatly on the~~ ~~measured data depends on the tunable~~ sediment grain size parameter, which controls subglacial sediment transport capacity. Smaller grain sizes allow sediment transport to occur in regions of the bed with  
15 reduced water flow and channel size, effectively increasing sediment connectivity into the main channels. ~~Model outputs from both cases show the importance of considering~~ ~~The model provides the essential components of modeling subglacial sediment discharge on seasonal to decadal timescales and reveals the importance of including~~ spatial heterogeneities in water discharge and sediment transport in both the  $x$ - and  $y$ - dimensions in evaluating sediment discharge ~~from glaciers.~~

## 1 Introduction

25 Increasing glacier ablation perturbs the ~~ways that~~ processes through which glaciers erode bedrock and supply sediment downstream (e.g., Church and Ryder, 1972; Lane et al., 2017; Delaney and Adhikari, 2020). Changing sediment discharge from glaciers in alpine and polar landscapes impacts many ~~downstream-~~ social and earth systems (Milner et al., 2017; Li et al., 2021). ~~In turn~~ Thus, predictive models are needed to understand the response of these systems to glacier retreat. In alpine environments, increased sediment discharge leads to the more rapid filling of proglacial reservoirs (Thapa et al., 2005; Li et al., 30 2022) and abrasion of hydropower infrastructure (e.g. Felix et al., 2016). The flux of sediment from glaciers also dramatically alters alpine ecosystems (Milner et al., 2017) ~~-In the Arctic occurs when high melt extends up-glacier, thus mobilizing sediment in new areas~~ (Lane et al., 2017; Delaney and Adhikari, 2020; Li et al., 2021). In Arctic environments, increased sediment discharge can affect biogeochemical cycles given that sediments may carry phosphorus and iron (Bhatia et al., 2013; Hawkings et al., 2014). These elements are limiting nutrients in the oceanic ecosystem, so any change to sediment discharge 35 from ~~the ice sheet can alter glaciers and ice sheets, therefore, alters~~ Arctic ecosystems (Wadham et al., 2019). ~~Modeling studies and observations suggest that increases in sediment output from alpine glaciers could occur when high melt extends up-glacier, mobilizing sediment in new areas~~ (Lane et al., 2017; Delaney and Adhikari, 2020; Li et al., 2021)-

Generally, two processes determine the sediment discharge below glaciers: one process adds sediment, and the other removes sediment from subglacial till layers (Figure 1; Brinkerhoff et al., 2017; Delaney et al., 2019). Bedrock erosion adds material 40 to the subglacial till layer. ~~Bedrock erosion~~ This is accomplished by quarrying, when pressure differentials on opposing sides of obstacles cause fractures to expand and rock to detach (Iverson, 1990; Alley et al., 1997; Hallet et al., 1996; Iverson, 2012), and by abrasion, when debris embedded in the ice grinds bedrock as the glacier slides above (Hallet, 1979; Alley et al., 1997). ~~Representing~~ Representation of these physical processes in models requires independent knowledge of a large number of parameters (c.f. Ugelvig et al., 2018), so many researchers use empirical relationships that relate glacier sliding to glacier 45 erosion (Humphrey and Raymond, 1994; Koppes et al., 2015; Herman et al., 2015; Cook et al., 2020). ~~The sliding relationship with glacier erosion proves~~ These relationships prove especially useful when applied over large temporal and spatial scales, for example, to explore the coupling of glacier erosion, climate, and tectonic uplift (e.g., Egholm et al., 2009; Prasicek et al., 2018; Herman et al., 2018; Prasicek et al., 2020; Seguinot and Delaney, 2021).

Conversely, fluvial sediment transport mobilizes material from subglacial till layers (~~e.g., Walder and Fowler, 1994; Ng, 2000; Creyts et al.~~ 50 ~~, or may deposit it there~~ (e.g., Walder and Fowler, 1994; Ng, 2000) or it may deposit the mobilized material in the till layers under certain hydraulic conditions (e.g., Beaud et al., 2018b). ~~When~~ (e.g., Beaud et al., 2018a; Hewitt and Creyts, 2019; Delaney and Andersson et al., 2020) As subglacial water velocity increases ~~above a critical threshold,~~ the sediment of a given grain size is transported ~~downglacier,~~ and if the water velocity slows below the threshold, below the glacier, and this sediment may be deposited (Shields, 1936). ~~The sediment if the water velocity slows~~ (e.g. Meyer-Peter and Müller, 1948; Paola and Voller, 2005). Sediment mobilization 55 ceases when no sediment is present, and the system is ~~supply-limited~~ (e.g., Mao et al., 2014). ~~It follows that~~ supply-limited (e.g., Mao et al., 2014). Thus, fluvial sediment transport depends on both the subglacial hydraulic characteristics (e.g., Walder and Fowler, 1994) ~~, and the~~ and the availability of sediment at the glacier bed (e.g., Willis et al., 1996; Swift et al., 2005).

Bedrock erosion and fluvial sediment transport vary depending on the characteristics of each glacier. Bedrock erosion processes tend to dominate sediment discharge below glaciers with minimal sediment storage, large concentrations of subglacial debris entrained at the glacier bed, and steep gradients (Hallet, 1979; Humphrey and Raymond, 1994; Herman et al., 2015; Ugelvig et al., 2018; Herman et al., 2021). Landscape evolution models that represent glacier landscapes illustrate the dominant role of erosional processes, as opposed to sediment transport processes, over geologic timescales (Harbor et al., 1988; Herman et al., 2011; Egholm et al., 2012). Over shorter timescales of months to decades, however, fluvial sediment transport often drives sediment discharge ~~from glaciers~~ (e.g., Delaney et al., 2018b; Perolo et al., 2018; Delaney et al., 2019).

65 The development of numerical models of subglacial sediment transport ~~has thus far to date has mainly~~ focused on processes acting ~~a single in the~~ downglacier (e.g.,  $x$ -) dimension. ~~Yet, the~~ To date, one-dimensional models have yielded insights into the creation of eskers (Beaud et al., 2018a; Hewitt and Creyts, 2019), the formation of subglacial canals through which water flows (Walder and Fowler, 1994; Ng, 2000; Kasmalkar et al., 2019), subglacial processes in overdeepenings (Creyts et al., 2013) and the behavior of tidewater glaciers (Brinkerhoff et al., 2017). ~~Yet~~ spatial heterogeneities in the distribution of sediment and sediment transport capacity (largely controlled by water velocity) ~~often result in less sediment being carried by the water commonly result in the water carrying less sediment~~ than could be transported theoretically (e.g., Lane et al., 2017; Delaney et al., 2018b) (e.g., Delaney et al., 2018b). As a result, reducing the ~~problem to one-dimension-modelled processes to one dimension~~ omits key processes controlling sediment dynamics because subglacial water flows through spatially distributed networks of cavities and channels across the glacier bed (e.g., Werder et al., 2013). ~~To date, the one-dimensional models have yielded insights into~~

75 ~~the creation of eskers (Beaud et al., 2018a; Hewitt and Creyts, 2019), the formation of subglacial canals through which water flows (Walder and Fowler, 1994; Ng, 2000; Kasmalkar et al., 2019), subglacial processes in overdeepenings (Creyts et al., 2013) and the behavior of tidewater glaciers (Brinkerhoff et al., 2017).~~ ~~Yet~~, Therefore, describing subglacial sediment transport inherently lends itself to a discretization of bedrock erosion, sediment transport, water flow, and sediment availability in both the downglacier and transverse dimensions (e.g.,  $x$ - and  $y$ -).

80 ~~In this manuscript~~Here, we present SUGSET\_2D, a two-dimensional subglacial sediment transport model. ~~The model includes subglacial that includes~~ sediment transport and bedrock erosion processes. We implement a routing scheme that transports sediment in  $x$ - and  $y$ - directions based on the local hydraulic potential gradient. Synthetic cases demonstrate the model's ability to reproduce known processes and yield ~~insight~~ insights into the spatially-distributed processes responsible for subglacial sediment dynamics. We also apply the model to a real alpine glacier, Griesgletscher ~~in Switzerland, in Switzerland,~~

85 which has a record of subglacial sediment transport from the catchment from the period 2011 to 2016. The model was run with ~~hydrology and topography data~~ topography data and modeled hydrology from the glacier, and measured sediment discharge data were used to validate the model. Through these experiments, we ~~explore the importance of two-dimensional sediment connectivity in the subglacial environment~~ identify key processes of sediment transport from subglacial environments.

## 2 Model Description

90 The model presented here implements a hydraulic model and sediment routing scheme that translates many of the underpin-  
nings of the one-dimensional subglacial sediment transport model presented in Delaney et al. (2019) to two dimensions. ~~In~~  
~~this section, we~~ We describe hydraulic and sediment transport models, explain the implemented water and sediment routing  
scheme, and outline its numerical implementation in two dimensions.

### 2.1 Hydraulic Model

95 SUGSET\_2D requires a hydraulic model as a means to route sediment and water through the subglacial environment. The  
hydraulic model ~~is also needed to evaluate~~ determines the sediment transport capacity of this the subglacial water, based upon  
the ~~hydraulic gradient~~ gradient of the hydraulic potential, channel size, and water flux (Table 1, Section 2.2; e.g., Walder and  
Fowler, 1994; Alley et al., 1997). The hydraulic model is based on the ~~premise assumption~~ that subglacial water flows along  
the hydraulic potential gradient ~~and~~, the weight of ice pressurizes water at the bed (Shreve, 1972), ~~and the channel size varies~~  
100 over a substantially longer time scale compared to water discharge. This model includes characteristics of ~~an a~~ Röthlisberger-  
channel without explicitly describing properties such as creep closure and pressure melt of channel walls (Röthlisberger, 1972)  
.

The ~~hydraulic gradient of~~ gradient of the hydraulic potential of a subglacial channel  $\Psi$  (at a certain location and time) can  
be determined with a known hydraulic diameter  $D_h$  ~~and (a function of channel size and shape) and~~ water discharge  $Q_w$ . The  
105 ~~hydraulic gradient~~ gradient of the hydraulic potential can then be determined using the Darcy-Weissbach equation for fluid  
flow through a pipe

$$\Psi = s f_r \rho_w \frac{Q_w^2}{D_h^5} w_c, \quad (1)$$

where the density of water is  $\rho_w$ , the Darcy-Weissbach friction factor is  $f_r$ , and the channel's cross-sectional geometry, which  
impacts water pressure, is accounted for by  $s$  (Hooke et al., 1990). We represent  $s$  as

$$s = \frac{2(\beta - \sin \beta)^2}{\left(\frac{\beta}{2} + \sin \frac{\beta}{2}\right)^4}, \quad (2)$$

110 where  $\beta$  is the central angle of the circular segment representing the channel edge. Smaller values of  $\beta$  result in broad channels  
and  $\beta = \pi$  results in a semicircular channel.

~~To approximate~~ We assume that the hydraulic diameter  $D_h$  ~~we prescribe a melt rate  $\dot{m}_w$  to establish  $Q_w$  and assign~~  
~~a representative of the channel results from a characteristic~~ water discharge  $Q_w^*$  ~~to  $Q_w$ , by taking a characteristic which is~~  
~~evaluated by the source percentile of~~ water discharge over a certain time period ~~prior (hours to days)~~. ~~We assume that the~~  
115 ~~hydraulic diameter of the channel results from this~~  $s_p$  and a response time of the channel size  $s_a$ , that remains consistent  
throughout the model run (Table 1; Delaney et al., 2019).

We sum the prescribed melt rate  $\dot{m}_w$  up the glacier to define  $Q_w$ , not considering englacial water storage. Percentile  $s_p$   
over a response time period prior to the timestep  $s_a$  is applied to  $Q_w$  to evaluate a characteristic water discharge we call the

source-percentile ( $s_p$ ; c.f. Gimbert et al., 2016; de Fleurian et al., 2018; Delaney et al., 2019; Nanni et al., 2020). The response time  $Q_w^*$  that represents the size of the conduit (hours to days; c.f. Gimbert et al., 2016; de Fleurian et al., 2018; Delaney et al., 2019; Nanni et al., 2020). The timescales,  $s_a$  and source-percentile,  $s_p$ , remain consistent throughout the model run. The values for these variables and characteristic water discharges ( $s_p$  and  $Q_w^*$ ), responsible for changes in subglacial conduit size are poorly constrained, yet their impact can be intuited. For instance, short-lived increases in water discharge due to an hour of precipitation will not greatly impact the hydraulic diameter of the subglacial channel, whereas prolonged melt would increase the hydraulic diameter.

$Q_w^*$  and  $Q_w$  comprise the total instantaneous amount of melt water produced upglacier, as this hydraulic model does not consider water storage. With data of representative water discharge below the glacier  $Q_w^*$  and the static hydraulic pressure gradient  $\Psi^*$ , a representative hydraulic diameter  $D_h$  can be estimated. For a short period, such a  $D_h$  is assumed time-independent and is defined in Equation 1.

$D_h$ , the hydraulic diameter is evaluated from

$$D_h = \left( s f_r \rho_w \frac{Q_w^{*2}}{\Psi^*} \right)^{\frac{1}{5}} . \quad (3)$$

$\Psi^*$  is a representative hydraulic gradient gradient of the hydraulic potential at overburden pressure, evaluated using the Shreve potential gradient

$$\Psi^* = \nabla(\rho_i g(z_s - z_b) + \rho_w g z_b) , \quad (4)$$

where  $z_s$  and  $z_b$  are surface and bed elevations, respectively,  $\rho_i$  is the density of ice and  $g$  is the gravitational acceleration constant.

With knowledge of  $D_h$ , we insert the instantaneous value of  $Q_w$  into Equation 1 to evaluate the instantaneous hydraulic gradient gradient of the hydraulic potential  $\Psi$ . To prevent unreasonable water pressures when  $Q_w^*$  rapidly increases and  $D_h$  is small, the model limits the minimal cross-sectional area  $S$  to  $0.5$  hydraulic diameter to  $0.3 \text{ m}^2$  (Delaney et al., 2019).

## 2.2 Till layer model: bedrock erosion and sediment transport

The model SUGSET\_2D simulates the evolution of a subglacial till layer, which we define as transportable sediment below the glacier due to produced through glacier erosion and fluvial sediment transport. Fluvial sediment transport, in supply- and transport-limited regimes, mobilizes and deposits sediment, adding or removing removing or adding material from the till layer (Brinkerhoff et al., 2017; Delaney et al., 2019). Conversely, erosive processes such as abrasion and quarrying add material to the layer, while till layer. Note that we do not consider processes such as fluvial abrasion that appear to produce minimal sediment (Beaud et al., 2018b). To represent these processes, we implement the Exner Equation (Figure 2; Exner, 1920a,b; Paola and Voller, 2005), a mass conservation relationship, to solve for the till layer height given the erosive and fluvial conditions.

$$\underbrace{\frac{\partial H}{\partial t}}_{\text{till evolution}} = - \underbrace{\nabla \cdot Q_s}_{\text{sediment transport}} + \underbrace{\dot{m}_t}_{\text{bedrock erosion}} , \quad (5)$$

145  $H$  is till thickness and  $t$  is time (Table 1). The first term represents fluvial sediment transport processes, where  $\nabla \cdot Q_s$  represents sediment mobilization ~~in either supply- or transport- limited regimes~~ or deposition. The second term captures bedrock erosion processes, where  $\dot{m}_t$  is a bedrock erosion rate.

We ~~evaluate the mobilization of sediment~~ calculate sediment mobilization in both supply- and ~~transport-limited~~ transport-limited conditions. Divergence of the sediment flux is evaluated by approximating  ~~$\nabla \cdot Q_s$  with  $\frac{\nabla \cdot \tilde{Q}_s}{w}$  and using the mobilization scheme~~  
 150 ~~from  $\nabla \cdot Q_s$  with  $\frac{\tilde{Q}_s}{w}$  using a similar mobilization scheme as in~~ Delaney et al. (2019)

$$\tilde{Q}_s = \begin{cases} \frac{Q_{sc} - Q_s}{l} & \text{if } \frac{Q_{sc} - Q_s}{l} \leq \dot{m}_t w & \text{(transport-limited)} & (6a) \\ 0 & \text{if } H = H_{lim} \quad \& \quad \frac{Q_{sc} - Q_s}{l} \leq 0 & (6b) \\ \frac{Q_{sc} - Q_s}{l} \sigma(H) + \dot{m}_t w (1 - \sigma(H)) & \text{otherwise} & \text{(supply-limited)} & (6c) \end{cases}$$

$\tilde{Q}_s$  is sediment mobilization across a width of the glacier bed  $w$  perpendicular to the water's flow direction. Note that  $w$  is not necessarily the channel width, but rather a representative width across the glacier bed over which sediment can be accessed by water flowing through the subglacial channel (Figure 2).  $Q_{sc}$  is the sediment transport capacity, or the or the maximum amount of sediment that could be transported under the given hydraulic conditions.  $l$  is a characteristic length-scale for sediment mobilization, over which sediment mobilization adjusts to sediment transport conditions.  $\sigma$  is a sigmoidal function of  $H$   
 155 mobilization, over which sediment mobilization adjusts to sediment transport conditions.  $\sigma$  is a sigmoidal function of  $H$

$$\sigma(H) = \left( 1 + \exp \left( \frac{2 - \Delta\sigma H}{5} \right) \right)^{-1}, \quad (7)$$

which enables a smooth transition from transport- to supply- limited transport in Equation 6c. If  $H$ , the till thickness, is greater than  $3 \Delta\sigma$ , then the impact on sediment mobilization is ~~unaffected-negligible~~ and the system is in a transport-limited regime. When  $H = \Delta\sigma$ , then  $\sigma(H)$  is close to 0, ~~and~~ sediment transport is in a supply-limited regime, and nearly no; no significant sediment mobilization takes place.

160 Condition 6a represents the case where bedrock erosion exceeds sediment mobilization, thus sediment transport exists in a ~~transport-limited~~ transport-limited regime. Condition 6b impedes mobilization or deposition, therefore transporting sediment to the next cell when a till thickness is equal to  $H_{lim}$ , the value of which is chosen to be on the order of the maximal change in till height over the model run ( $\sim 10$  cm). This term Condition 6b prevents unbounded sediment accumulation, as the model does not include physical processes to limit sediment deposition, such as reduced channel size and increased water velocity  
 165 in response to the infill of sediment (Perolo et al., 2018). Condition 6c allows sediment mobilization to transition between transport- and supply-limited regimes, limiting sediment mobilization to the sediment production term,  $\dot{m}_t$  (see below), when  $H$  is small and thus minimal sediment is available for transport. With ~~these three conditions, we can evaluate~~ Conditions 6a, 6b, and 6c, we can calculate sediment transport in transport- and supply-limited regimes and pass sediment through the system ~~when till height is large.~~

170 We calculate sediment transport capacity  $Q_{sc}$  using the total sediment transport relationship by Engelund and Hansen (1967),

$$Q_{sc} = \frac{0.4}{f_r} \frac{1}{D_m \left( \frac{\rho_s}{\rho_w} - 1 \right)^2 g^2} \left( \frac{\tau}{\rho_w} \right)^{\frac{5}{2}} \underline{w_c}, \quad (8)$$

where  $\rho_s$  ( $\rho_w$ ) is the bulk density of the sediment (water),  $D_m$  is the mean sediment grain size and  $\tau$  represents the shear stress between the water and the channel bed.

The width of the channel floor  $w_c$ , ~~needed~~ required to evaluate the surface ~~over which~~ over which sediment transport may occur, is given by

$$w_c = 2 \sin \frac{\beta}{2} \sqrt{\frac{2S}{\beta - \sin \beta}} , \quad (9)$$

where ~~again~~, again,  $\beta$  is the Hooke angle controlling channel morphology (Section 2.1), and  $S$  is the cross-sectional area of the channel given by

$$S = \frac{D_h^2}{2} \frac{\left(\frac{\beta}{2} + \sin \frac{\beta}{2}\right)^2}{\beta - \sin \beta} . \quad (10)$$

Here, hydraulic diameter  $D_h$  is evaluated from Equation 3.

We also determine the shear stress ~~through the~~ between water flowing through the channel and the sediment below in Equation 8 through the Darcy-Weisbach relationship

$$\tau = \frac{1}{8} f_r \rho_w v^2 , \quad (11)$$

where  $v = \frac{Q_w}{S}$  is the water velocity. Water discharge  $Q_w$  is calculated by the water flowing above a position in the glacier and  $S$ , the cross-sectional area, is evaluated in Equation 10. Other sediment transport relationships using shear stress could be exchanged by the model operator (e.g., Meyer-Peter and Müller, 1948). We ~~chose~~ have chosen Engelund and Hansen (1967)'s formulation due to the representation of both suspended and bedload transport.

We assume that till armors the bed from erosion (e.g., Alley et al., 2003; Brinkerhoff et al., 2017; Delaney et al., 2019). In response, the source term,  $\dot{m}_t$ , is described as

$$\dot{m}_t = \dot{e} \left(1 - \frac{H}{H_{max}}\right) , \quad (12)$$

where  $H_{max}$  is a till height beyond which no further erosion,  $\dot{e}$ , may occur.

We ~~chose to~~ use an empirical relationship with sliding velocity  $u_b$  to describe bedrock erosion,

$$\dot{e} = k_g u_b^{l_{er}} , \quad (13)$$

where  $k_g$  is an erodability constant and  $l_{er}$  is an exponent, which varies from between 0.66 and 3 (Herman et al., 2021). The sliding velocity,  $u_b$ , is assumed to be related to basal shear stress ( $\tau_b$ ; Weertman, 1957) given the following relationship,

$$u_b = B \tau_b^m , \quad (14)$$

where  $B$  is a constant and we assume the exponent  $m$  is equal to 1.

We assume that  $\tau_b$  is equal to driving stress (Cuffey and Paterson, 2010)

$$\tau_b = \rho_i g h \sin(\alpha) , \quad (15)$$

where  $\rho_i$  is the density of ice,  $h$  is the glacier thickness, and  $\alpha$  is the surface slope of the glacier.

Note that alternative parameterizations of erosion or basal sliding can easily be exchanged for  $\dot{m}_t$ .

~~Here, we describe the~~ We describe the water and sediment routing and numerical implementation of the equations presented above, ~~and in particular the routing scheme that enables a two-dimensional representation of subglacial fluvial and till dynamics.~~

### 2.3.1 Water and sediment routing and implementation

200 ~~We assume that~~ A routing scheme is implemented to 1) evaluate the hydraulic potential and thus the direction of the water flow and 2) transport sediment and water ~~moves~~ across the glacier bed ~~following the steepest gradient in hydraulic potential.~~ On glaciers, we define, to where it is expelled or deposited.

To evaluate the hydraulic potential ~~at a cell  $i$  in the grid,  $\phi_i$ ,~~ based upon the elevation of the glacier bed plus the ice thickness, ~~following Shreve (1972).~~

205 
$$\phi_i = f_f \rho_i g (z_{s,i} - z_{b,i}) + \rho_w g z_{b,i} ,$$

~~where  $f_f$  is the flotation fraction and thus the direction of the water and sediment flow~~ across the glacier bed,  ~~$z_s$  is the glacier surface, and  $z_b$  is the glacier bed.~~

~~With this information,~~ we use a multi-cell two-dimensional routing scheme (Quinn et al., 1991) to establish flow routing based upon on the steepest hydraulic potential ~~in Equation 16 and with a single value of  $f_f$  across the glacier bed.~~ We implement  
210 this scheme in a similar way as fashion to Bovy et al. (2016), but on a regular grid with square cells, extending in  $x$  and  $y$  directions, ~~where~~. Water and sediment fluxes can pass to the four surrounding cells sharing an edge, as a result of the  $x$ - and  $y$ - components of the hydraulic gradient at a given point in time. This routing scheme algorithm returns a stack ( $s_i$ ; Table 3), which is a vector that contains information about the order of cells to perform the calculations, along with the number of cells flowing in-to-into a cell (donors;  $n_d$ ), the number of cells that a to which a single cell contributes (receivers;  $n_r$ ), and the weight  
215 or the percentage of hydraulic potential and water ~~or sediment (or sediment)~~ discharge directed from one cell to another ( $w_d$  or  $w_r$ ), as determined by the hydraulic potential gradient between cells (Figure 4).

~~For the first~~ We define the hydraulic potential, upon which the routing scheme is evaluated, at a cell  $i$  in the grid,  $\phi_i$ , based upon the elevation of the glacier bed plus the ice thickness, following Shreve (1972)

$$\phi_i = f_f \rho_i g (z_{s,i} - z_{b,i}) + \rho_w g z_{b,i} , \quad (16)$$

where  $f_f$  is the flotation fraction across the glacier,  $z_s$  is the glacier surface, and  $z_b$  is the glacier bed.

220 For the initial time step, the hydraulic potential  $\phi$  is evaluated under the condition that  $f_f = 1$ . After the first time step, we assume that the flotation fraction  $f_f$  will vary in response to changing hydraulic conditions, such as diurnal or seasonal water input (e.g., Iken and Bindshadler, 1986). In turn, to establish an average flotation fraction,  $f_f$  across the glacier bed for Equation 16, we use

$$f_f = \text{mean} \left( \frac{\phi_{o,i}}{\rho_i g (z_{s,i} - z_{b,i}) + \rho_w g z_{b,i}} \frac{\phi_{0,i}}{\rho_i g (z_{s,i} - z_{b,i}) + \rho_w g z_{b,i}} \right) , \quad (17)$$



where the denominator represents the hydraulic potential at ~~overburden pressure~~ the overburden pressure of the glacier ( $f_f = 1$  in Equation 16), and  $i$  represents a cell in the grid.

$\phi_0$  represents the hydraulic potential evaluated from summing the ~~hydraulic gradient~~ gradient of the hydraulic potential,  $\Psi$ , in Equation 1 up glacier ~~from its outlet~~.  $\phi_0$  at each cell  $i$  is evaluated as

$$\phi_{o,i} = \Psi_{i,j} \cdot \lambda + \sum_{j=1}^{n_r} (\phi_{0,j} \cdot w_{r,j,i,j}) . \quad (18)$$

Here,  $\Psi$  ~~comes from by~~ evaluating Equation 1 ~~from the~~,  $\Psi_{i,j}$  is established for receiver cell  $j$  of  $i$ ,  $\lambda$  is the edge length of a cell on a regular grid,  $n_r$  is the number of receivers that the cell  $i$  has, and  $w_{r,j,i,j}$  is the proportion of the hydraulic potential fed by the upstream cell  $j$  to cell  $i$ . The operation is executed on a cell-by-cell basis, beginning at the base of the glacier with cells that have no receivers, such as those near the glacier terminus, and moving up the flow paths evaluated in the routing scheme glacier using the inverted stack in  $s_t$  (Figure 4).

Using the routing scheme above, ~~but performing the operation from the top of the glacier~~, we evaluate the water discharge in a cell from cell  $i$ ,  $Q_{w,i}$ , from melt upstream as

$$Q_{w,i} = w_{w,i} \cdot \delta + \sum_{j=1}^{n_d} Q_{w,j} \cdot w_{d,j,i,j} + \dot{m}_{w,i} \cdot \delta , \quad (19)$$

where  $\dot{m}_w$  is a prescribed meltwater source term in cell  $i$ , where  $n_d$  is the number of cells directing water at donor cells for cell  $i$ , and  $w_{d,j,i,j}$  is the percentage of water flow from cell  $j$  directed at to cell  $i$ , and  $\dot{m}_{w,i}$  is a prescribed meltwater source term in cell  $i$ . The operation begins with cells that have no donors (for instance at the top of the glacier), so that water accumulates down the glacier (Figure 4).

Sediment mobilization into a cell  $Q_{s,i}$  is like-wise. The amount of sediment leaving a cell  $i$ ,  $Q_{s,i}$ , is the flux into the cell plus the sediment mobilized in the cell, which is defined as

$$Q_{s,i} = \sum_{j=1}^{n_d} Q_{s,j} \cdot w_{d,i,j} + \tilde{Q}_{s,i} \cdot \lambda . \quad (20)$$

The first term is the flux of sediment into the cell  $i$  from donor cells  $j$ . The second term is sediment mobilization,  $\tilde{Q}_{s,i}$  in cell  $i$ , which is computed by implementing Equation 6 from the top of the glacier through the stack as as

$$\tilde{Q}_{s,i} = \begin{cases} \sum_{j=1}^{n_d} \left( \frac{Q_{sc,j} - Q_{s,j}}{l} \cdot w_{d,i,j} \right) & \text{if } \sum_{j=1}^{n_d} \left( \frac{Q_{sc,j} - Q_{s,j}}{l} \right) \cdot w_{d,i,j} \leq \dot{m}_{t,i} \cdot \lambda \sum_{j=1}^{n_d} \left( \frac{Q_{sc,i,j} - Q_{s,i}}{l} \right) \\ 0 & \text{if } H_j = H_{lim} \ \& \ \frac{Q_{sc,j} - Q_{s,j}}{l} \leq 0 \ H_j = H_{lim} \ \& \ \frac{Q_{sc,i}}{l} \\ \frac{\dot{m}_{t,i} \lambda}{n_d} (1 - \sigma(H)) + \sum_{j=1}^{n_d} \left( \frac{Q_{sc,j} - Q_{s,j}}{l} \right) \cdot \sigma(H) \cdot w_{d,i,j} & \text{otherwise} \end{cases}$$

where  $Q_{sc,j}$  is the sediment transport capacity from cell  $j$  flowing to  $i$ ,  $Q_{s,j}$  is sediment discharge entering from cell  $j$  to cell  $i$ , again  $l$  is a response length scale, and  $\lambda$  is cell edge length.

Sediment discharge  $Q_{s,i}$  out of a cell  $i$  is evaluated as-

$$Q_{s,i} = \overline{Q_{s,i}} \cdot \lambda + \sum_{j=1}^{n_d} Q_{s,j} \cdot$$

245 We evaluate the change in till height at a cell by implementing Equation 5 as

$$\frac{dH_i}{dt} = \frac{-Q_{s,i} + \sum_{j=1}^{n_d} Q_{s,j}}{\delta} - \frac{Q_{s,i} + \sum_{j=1}^{n_d} Q_{s,j} \cdot w_{d,i,j}}{\delta} + \dot{m}_{t,i} \quad , \quad (22)$$

where ~~again~~  $\delta$  is ~~cell area~~. the cell area (Figure 4). The term,  $Q_{s,i}$  is the amount of sediment leaving the cell from Equation 20, and the term,  $\sum_{j=1}^{n_d} Q_{s,j} \cdot w_{d,i,j}$  is the sediment flux entering the cell from the donors.

### 2.3.2 Numerics and parameters

Spatial discretization on the regular grid must be substantially smaller than characteristic length-scale,  $l$ , in Equations 6 and 21.

250 We then solve Equation 22 to establish till height,  $H$ , for given initial and boundary conditions in response to till production,  $\dot{m}_t$  and, and the divergence of the sediment discharge,  $Q_s$  using an explicit time integration scheme.

To discretize the problem in time, the model implements the VCABM solver (Hairer et al., 1992; Radhakrishnan and Hindmarsh, 1993) from the package *DifferentialEquations.jl* (Rackauckas and Nie, 2017) to evolve till layer height,  $H$ . This solver implements an adaptive time step and uses a linear ~~multistep method (Adams-Moulton)~~ Adams-Moulton multistep method that  
 255 is well-suited to non-stiff problems, which is optimal because of the rapid fluctuations in sediment transport that can occur. We impose a maximum time step of 6 h to ensure that the model captures the response to diurnal variations in melt input. In practice, the solver commonly uses a time step of roughly 20 minutes, which varies depending on sediment transport conditions and solver tolerance. Longer time steps occur over periods ~~when with minimal~~ glacier melt, and thus sediment transport ~~ceases~~ ceases (i.e. winter months). Table 3 presents the numerical parameters used.

260 We execute the routing scheme based upon hydraulic conditions to the nearest 6 minutes to improve stability and fill closed basins in the hydraulic potential to maintain continuous sediment transport through the domain. Smaller solving tolerances increase the computational time due to 1) the increased accuracy of the solution and 2) the reassessment of flow fractions between the adjacent cells, which results in different routing configurations as the model converges.

We impose boundary conditions on the edge cells so no sediment or water enters the domain. At outlet cells, water discharge  
 265 leaves the domain, as does a flux of sediment, based on sediment transport conditions. In other applications, boundary conditions could also be set to represent processes ~~such as~~ hillslope erosion or glacial lakes, ~~that which~~ route sediment or water to the subglacial environment (e.g., Andersen et al., 2015). At the outlet cells, we assume that the hydraulic potential has no ice overburden pressure.

Evolving Equation 5 requires an initial till height,  $H_0$ , chosen by the model user. This initial till height represents material  
 270 from bedrock erosion created prior to the model initialization. We apply a “spin up” procedure to create a reasonable relationship between the amount of fluvial sediment transport and bedrock erosion.

New versions of the code are tested against reference cases to ensure consistency. Additionally, in each test, we ensure mass conservation by ~~checking~~ verifying that the amount of sediment leaving the system through fluvial transport is consistent with the till height change and erosion occurring under the simulated glacier.

## 275 3 Model Application

We use two ~~eases~~ case studies to highlight model viability under increasingly complex situations. First, we apply the model to a synthetic alpine glacier topography with a synthetic hydrologic forcing, based on the Subglacial Hydrology Model Inter-comparison Project (SHMIP; de Fleurian et al., 2018), to illustrate the model's performance in a simplistic scenario. We then apply the model to the topography, ~~and~~ sediment and water discharge at Griesgletscher in the Swiss Alps. We demonstrate  
280 ~~the proficiency of the model by comparing sediment transport model output and its~~ proficiency by comparing the calculated sediment transport output with measured data (Delaney et al., 2018a). We also identify ~~some drivers of important factors~~ controlling subglacial sediment discharge in ~~the model from~~ these simulations.

### 3.1 Synthetic alpine ~~eases~~ case

#### 3.1.1 Experiment design

285 We run simulations using ~~an a~~ synthetic alpine glacier geometry, along with ~~the~~ seasonally and diurnally varying hydrological forcing from the SHMIP project experiments (de Fleurian et al., 2018)). The domain is 6000 m on one axis and 1080 m on the other (Figure 7). The resulting geometry approximates the Bench Glacier in Alaska. The U-shaped bed and variable ice thickness mean that variable hydrologic gradients will occur ~~laterally across the glacier and water can be~~ perpendicular to the flow, thus water and sediment are routed across multiple cells.

290 To represent ~~hydrology that varies over a~~ hydrological environment that varies both seasonally and diurnally, we implement a simple spatially distributed melt model, as in SHMIP ( de Fleurian et al., 2018)

$$\dot{m}_w(z_s) = \begin{cases} M_f T(z_s) + \dot{m}_b & \text{if } T(z_s) > 0 \\ \dot{m}_b & \text{if } T(z_s) \leq 0 \end{cases}, \quad (23)$$

where  $M_f = 0.01 \text{ m } \underline{\text{K}} \text{C}^{-1} \text{ d}^{-1}$  is a melt factor, and  $\dot{m}_b$  is the basal melt rate.  $T(z_s)$  is air temperature  $T$  C at elevation  $z_s$ , defined as

$$295 \quad T(z_s) = \left( -A_a \cos\left(\frac{2\pi t}{s_{year}}\right) + A_d \cos\left(\frac{2\pi t}{s_{day}}\right) + \Delta T - 5 \right) \cdot \left( 1 + z_s \frac{dT}{dz} \right), \quad (24)$$

where  $A_a$  and  $A_d$  are the annual and diurnal amplitudes in temperature, respectively;  $\Delta T$  is a temperature offset ~~,-which that~~ is adjusted to control the meltwater input;  $s_{day}$  are the number of seconds in one day;  $s_{year}$  is the number of seconds in a year;  $\frac{dT}{dz} = -0.0075 \text{ K m}^{-1}$   $\frac{dT}{dz} = -0.0075 \text{ C m}^{-1}$  is the air temperature lapse rate (de Fleurian et al., 2018). In this case, we route

water directly to the subglacial system at the location where the melt occurs, ~~for instance,~~ omitting moulins or crevasses that concentrate meltwater delivery to the bed, for instance.

We run the model for 10 years with a steady climate, ~~then we;~~ we then apply a linear temperature increase of  $0.5^{\circ} \text{ a}^{-1}$  for 10 years followed by 10 years of steady temperature at the maximal  $\Delta T$ . We implement ~~the~~ this dramatic warming to capture the model's ~~response to variable ability to represent different~~ climatic conditions. The model is initiated with 5 cm of till across the bed. To spin up the model, we apply the initial year of hydrological forcing for 5 a ~~for computational reasons to~~ limit computational time. In other applications ~~the spin-up;~~ the spin-up could be maintained, until the annual change in till height was well below commonly accepted glacier erosion rates (Hallet et al., 1996).

### 3.1.2 Model outputs and findings

~~Simulations~~ The simulations show that over seasonal timescales, sediment discharge increases at the onset of melt and decreases shortly thereafter, but prior to the maximum amount of water discharge that occurs ~~in at~~ the peak of each melt season (Figure 5). ~~Daily-averaged sediment discharge decreases~~ Maximum and average quantities of daily sediment discharge decrease until the very end of the melt season, when sediment discharge increases very slightly again (~~Figure~~ Figures 5 and 6 b, d, f). This slight increase occurs when water stops flowing during the night, allowing sediment ~~to from bedrock erosion to~~ briefly accumulate in the channels from bedrock erosion. Increased sediment discharge produced by the model at the beginning of the melt season results from greater sediment availability following the growth of the till layer over the winter months ~~;~~ when the small amount of melt prevents substantial transport ~~sediment.~~ Increases of sediment. In fact, similar increases in sediment discharge have been observed in alpine glaciers at the onset of melt ~~produced by the model each season~~ (Figure 5 b, and 6 b, d, f) ~~have been observed for real glaciers (Willis et al., 1996; Swift et al., 2005; Riihimaki et al., 2005; Delaney et al., 2018b) and (Willis et al., 1996; Swift et al., 2005; Riihimaki et al., 2005; Delaney et al., 2018b) and are reproduced in the one-dimensional version of this model (Delaney et al., 2019) the model in Delaney et al. (2019).~~

Over the course of the simulation, the mean till height ~~continues to decrease~~ across the glacier generally decreases throughout the model run, although there are small increases in till height during the winter months without sediment transport and larger decreases in till height during the time periods with substantial melt (Figure 5 a and 6 a, c, e). Exhaustion of sediment is evident in the middle of the glacier where much of the water flows ~~resulting from the spin-up procedure,~~ as a result of the spin-up procedure, prior to the model initialization (Figure 7 e, f). ~~However,~~ Note that the decreasing till height through the model run results from sediment mobilization on the margins of the glacier, where water flow increased water flow occurs more often in a warmer climate ~~occurs more often. Increased water flow.~~ During the climate warming from years 10-20, sediment discharge from the glacier increases due to greater melt and water discharge on the upper reaches of the glacier. This results in increased sediment transport at higher elevations on the glacier, where sediment could persist in a cooler climate (Figure 5 b) ~~and a greater area of the bed where sediment transport occurs~~ e, f). Following the stabilization of the climate at year 20, sediment discharge remains elevated compared to the cooler climate because sediment transport occurs over a larger region of the glacier bed (Figure 7 e, fb).

~~For the cases described above~~In the model, bedrock erosion relies only on driving stress and till thickness. Sliding and bedrock erosion did not vary seasonally with increased subglacial water discharge (Figure 5 a). This causes sediment to accumulate during the winter months, which subsequently provides ample material for transport when ~~melt~~melting increases in the spring. To test the effects of spatially variable erosion and the role of hydrology, we present two additional cases to supplement the synthetic alpine glacier case above, named ORIGINAL. ~~One additional~~In an additional synthetic case, SEASON, simulates bedrock erosion by only allowing sliding, and thus erosion, during the summer months (~~e.g., Iken and Bindshadler, 1986~~) (e.g., Iken and Bindshadler, 1986; Herman et al., 2011); the same ~~erosion-erosional~~ relationship is applied as ~~the case that~~ in Section 3.1 ~~.In this~~(Equations 13 and 12). In the SEASON case, however, erosion ~~only occurs~~occurs only when the amount of water input substantially exceeds the background basal melt input rate  $\dot{\tau}$  that is present in the winter. ~~We choose this case to capture~~This case captures the seasonal variations in bedrock erosion (Ugelvig et al., 2018). In ~~the other~~another additional case, CONST, bedrock erosion remains constant over the entirety of the glacier at a rate of  $2 \text{ mm a}^{-1}$ , independent of ~~the spatially varying~~ glacier sliding velocity ~~of the other cases~~ (Figure 7).

The ORIGINAL case discharges over  $11,620 \text{ m}^3$  of sediment per year, while the SEASON case discharges only 60% of that value due to the absence of bedrock erosion during the winter months. The CONST case discharged  $7320 \text{ m}^3$  of sediment over the year ~~.CONST's~~or 63% of the ORIGINAL case. The quantity of sediment discharge in the CONST case results in a catchment-scaled height change ~~roughly in the till layer of approximately~~  $1.1 \text{ mm a}^{-1}$  due to decreased erosion efficiency with till height (Equation 12), instead of ~~the~~ prescribed bedrock erosion rate of  $2 \text{ mm a}^{-1}$  (Equation 12). Additionally, the spatial disparity of where sediment is produced at the glacier bed compared to the location of sediment transport further reduces the catchment scaled height change (Figure 7 e, f).

~~Over the three~~In each of the three synthetic cases, sediment discharge increases at the onset of melt and substantially decreases by the end of the melt season, due to sediment exhaustion (Figure 7). In ORIGINAL (Figure 6 a, b), ~~more~~greater sediment discharge occurs compared to the alternate cases (SEASON and CONST). The increased sediment discharge in ORIGINAL ~~is results from~~ 1) ~~due to the prolonged period~~the winter periods without melt over which bedrock erosion ~~occurs adding~~ adds more sediment to the layer in the absence of sediment transport and 2) ~~because bedrock erosion~~bedrock erosion that occurs low on the glacier where much ~~sediment transport takes place~~of the sediment transport occurs (Figure 7 d); ~~compared to~~. By contrast, in the CONST case, where a steady amount of erosion occurs across the entire glacier bed. The peak sediment discharge in CONST (Figure 6 e, f) occurs slightly earlier in the season ~~compared to ORIGINAL and SEASON cases~~, due to the increased amounts of sediment ~~on~~below the glacier's lower portions.

## 360 3.2 Griesgletscher

### 3.2.1 Experiment design

We also ~~simulate~~run simulations of Griesgletscher in the Swiss Alps using topographic data from Delaney et al. (2019). ~~Hourly water discharge from the glacier was modeled in Delaney et al. (2018a)~~. Here, we ~~use the~~run the model from 2009-2017, ~~with the modeled water~~ discharge time series from 2009-2017 (Delaney et al., 2018a). Subglacial sediment discharge from the

365 glacier ~~was determined for~~ is determined over four different time periods ~~since fall 2011 by differencing bathymetry maps~~ (2011 - 2013, 2013 - 2014, 2014 - 2015, 2015 - 2016) by differencing the bathymetry maps collected through this period and considering proglacial erosion quantities ~~(Delaney et al., 2018a)~~ (Delaney et al., 2018a, 2019). To estimate surface melt across the glacier with respect to elevation, we use  $\bar{\tau}$

$$\dot{m}_w(x, y) = \dot{b}^0 + \gamma(z_s(x, y) - z_s^0). \quad (25)$$

370 Here,  $\gamma$  is the mass balance gradient ~~and~~;  $z_s^0$  represents the glacier's lowest elevation ~~,~~ and  $\dot{b}^0$  represents the melt rate at the glacier's lowest extent.  $\dot{b}^0$  was evaluated numerically at each water discharge value using the hypsometry of the glacier.

We apply a parameter search over a range of values of sediment grain size ( $D_m$ , representing a primary control on fluvial transport of subglacial sediment), sliding rate factor ( $B$ , representing a control on bedrock erosion), and the initial till height condition ( $H_0$ , representing the effects of existing quantities of sediment below the glacier). 100 simulations were run with randomly selected parameters ~~,~~ each with from a uniform distribution. No ~~spin-up~~ spin-up was applied in this case to establish an initial condition, because of the wide range of  $H_0$  values explored.

The wall time for a single model run averaged 8.9 h, and each run for a parameter set was executed on a single CPU. Instead of applying the mean flotation fraction across the glacier, as ~~was~~ done in the ~~previous~~ synthetic cases, the maximum value was applied with an upper limit of 1.

380 We ~~only considered~~ consider model outputs resulting in a perfect rank correlation across the four data collection periods and ~~an error less than~~ have errors less than the  $131,000 \text{ m}^{-3}$  of sediment that was expelled from the glacier over this period (Delaney et al., 2018a, 2019). For the ~~case example~~ presented below, we show the simulation with the lowest absolute error between the model output and the sediment transport data.

### 3.2.2 Model outputs and findings

385 The parameter search yields an optimum grain size parameter  $D_m$  of 2 cm, sliding parameter  $B$  of  $2.05 \times 10^{-11} \text{ MPa m s}^{-1}$  and initial till height  $H_0$  of 2.5mm (see red stars, Figure 8 a, b, c). The model's ability to reproduce the quantities of sediment in the validation data largely depends on the grain size parameter,  $D_m$ , shown by Figure 8 a. Compared to  $D_m$ , the sliding parameters ( $B$ ) and initial condition parameters ( ~~$B$  and~~  $H_0$ ) have a reduced influence in representing the measured data, given that similar values of  $B$  and  $H_0$  can produce largely different ~~results~~ model outputs in the context of  $D_m$  (Figure 8 a, b, c).

390 The optimized ~~model parameter combination, along with other parameter combinations,~~ reproduces the interannual variability in sediment discharge from the Griesgletscher (Figure 8 g). The absolute error between the ~~model and the measurements~~ optimum model run and the measured data is roughly  $62,600 \text{ m}^3$  of sediment. The error ~~from this parameter search~~ is slightly less than half of the  $131,300 \text{ m}^3$  total sediment discharged from the Griesgletscher over this time period (Delaney et al., 2018a) ~~.~~ The model runs captures from 2011 to 2016 (Delaney et al., 2018a). In fact, the model runs capture the third period from late 2014 to late 2015 well. However, the runs systematically overestimate the second and fourth periods and generally underestimate the high sediment discharge period from late 2011 until late 2013 (Figure 8 g).

The ~~best-performing~~ best-performing model run shows strong temporal variability in sediment discharge ~~Peaks~~ (Figure 9 a). Some of the peaks in sediment discharge occur during the ~~short-lived~~ short periodic increases in water discharge. Yet the greatest sediment discharge values do not necessarily occur at the highest water discharge values (Figure 9 a and Figure 10 a).  
400 Despite the strong dependence on grain size and fluvial transport of sediment in the parameter search ~~(Figure 8 a)~~, the modeled sediment transport capacity  $Q_{sc}$  still remains roughly an order of magnitude higher than the calculated sediment discharge  $Q_s$  (Figure 9 a, b). The steep section of the glacier (Figure 11 c) experiences sediment depletion over the model run, as do several patches of the glacier bed near the over-deepening and high on the glacier (lower left of panels in Figure 11 c d). On some parts of the upper glacier, the calculated bedrock erosion grows the till layer beyond the initial condition in the absence of substantial  
405 sediment transport.

The ~~value of~~ range of values for  $B$ , ~~from the~~ the sliding parameter, in the parameter search, ~~results in an average sliding velocity of~~  $39 \text{ m a}^{-1}$ , ~~and the range of values for~~  $B$  in the parameter search result search results in mean sliding velocities roughly across the glacier between  $14 \text{ m a}^{-1}$  and  $70 \text{ m a}^{-1}$  (Equation 14). ~~Because sediment production decreases with till height (Equation 12), sediment production~~ The optimum run in the parameter search results in an average sliding velocity of  
410  $39 \text{ m a}^{-1}$ . We note that smaller sliding velocities could result in equivalent amounts of erosion if the parameters  $k_g$  and  $l_{er}$  in Equation 13 are increased. The model reveals that the relatively large velocities needed to produce adequate amounts of erosion occur in part because sediment production in the model, is limited to the narrow patches of the glacier bed where minimal till persists and bedrock erosion may occur. As a result, the model requires more sliding to produce the equivalent amount of sediment with more till at the bed, even though the sliding and erosion parameters applied here are within a ~~well-constrained~~  
415 ~~range~~ reasonable range (Figure 11 c d).

#### 4 Model limitations

The lack of ~~knowledge regarding observations of~~ the spatial distribution of subglacial sediment makes selecting an initial value of  $H$ , the height of the till layer, difficult. The slow rate of basal erosion ~~means~~ suggests that an equilibrium between fluvial sediment transport and bedrock erosion will likely take centuries to attain ~~if such an equilibrium may~~ could even exist in light  
420 of ~~variable~~ the variability in climatic, and thus glacier, conditions. Should an equilibrium eventually be present (e.g., Herman et al., 2018; Delaney and Adhikari, 2020), it is probably ~~outside of~~ beyond a feasible computational time ~~of this model given its current for this model, given its~~ processing speeds.

In addition to selecting an initial value of  $H$ , we also SUGSET 2D also contains 20 parameters (Table 2 and 3). In the available literature, some of these parameters have been partially constrained using inverse methods (Brinkerhoff et al., 2016)  
425 as well as detailed modeling and measurements (e.g., Chen et al., 2018; Covington et al., 2020; Pohle et al., 2022). However, many are poorly constrained.

For instance, we limit the thickness at which the till layer must stop accumulating sediment (Equation 6b,  $H_{lim}$ ) due to the changes in the hydraulic potential caused by channel infill of sediment. We assume that this value is on the order of tens of centimeters (Table 2), based upon available observations of sediment deposition and glacier uplift (Perolo et al., 2018). While

430 the impact of a till layer on bedrock abrasion remains uncertain, we expect that sediment of a certain thickness will armor the bed, preventing erosion (Alley et al., 2003). In turn, we limit erosion with till thickness to a threshold (5 cm), of the same order as  $H_{lim}$  to improve computational time. ~~Additionally, the model~~ Due to the difficulty of making direct observations at glacier beds, only one study, to our knowledge, has quantified till thickness at a single point below a glacier (Truffer et al., 2000). The initial till height,  $H_0$ , in the model, therefore, must be chosen thoughtfully because the system will remain impacted by  
435 this boundary condition throughout the model run. Furthermore, the model does not consider the interactions between fluvial sediment transport ~~and~~, debris concentrations in subglacial ice, and bedrock erosion, which may be important for ~~sub-glacial~~ subglacial sediment transport (e.g., Ugelvig et al., 2018).

~~SUGSET\_2D also contains 20 parameters (Table 2 and 3). In the available literature, these parameters have been partially constrained using inverse methods (Brinkerhoff et al., 2016) as well as detailed modeling and measurements (e.g., Chen et al., 2018; Covington et al., 2018).~~

440 -

The routing method we use assumes that the water flow direction is in response to the Shreve potential (Section 2.3.1). Therefore, it does not explicitly simulate the evolution of efficient and inefficient subglacial drainage systems, over the course of the season, ~~or nor~~ the inheritance of existing subglacial canals or channels (Figure 3; e.g., Werder et al., 2013; Zechmann et al., 2020). ~~Furthermore~~ In addition, a response time of the subglacial channel is chosen prior to simulation ~~to improve~~ computational time; ~~this could be~~ compared to a more sophisticated, but computationally more expensive, representation of processes in an R-channel model (e.g., Röthlisberger, 1972).

445

## 5 Implications

Results of ~~both~~ the one-dimensional model (SUGSET; Delaney et al., 2019) and the two-dimensional model, SUGSET\_2D, highlight the importance of simulating the spatial heterogeneities in bedrock erosion, sediment availability, and sediment  
450 transport capacity. ~~Yet, in~~ In the one-dimensional version of SUGSET, ~~sediment can be accessed~~ water can access sediment from the till layer across the entire glacier width, perpendicular to the glacier flow line. In SUGSET\_2D, however, sediment access and transport are not averaged over the glacier width. Rather, by considering the spatial distribution in water discharge and sediment availability laterally below a glacier, the model evaluates where heterogeneities may persist and ~~their impact on~~ how these heterogeneities will impact subglacial sediment dynamics (Figures 7 ~~and~~ 11).

455 In SUGSET\_2D, large diurnal increases in sediment discharge occur near peak daily melt because the area of flowing water expands under the glacier (Figure 6 b, d, f). As a result, increased sediment transport can occur in regions of the glacier bed with substantial sediment when hydraulic conditions permit, ~~then the~~; that patch of bed is abandoned when water is routed to another part of the glacier bed (Video supplement). This allows sediment to be stored in these regions of the bed until the hydraulic conditions return and ~~increased~~ renew the increase in sediment transport. Such ~~a process is difficult to represent~~ processes cannot be represented in a one-dimensional model, where the entire width of the glacier ~~is represented~~ evolves together (Figures 5 b and 6 b, d, f; ~~Video supplement~~). ~~For instance here, diurnal fluctuations in sediment discharge in the middle of the season can be 50% above the mean value (Figure 6 b, d, f), which aligns more closely with some field observation~~

460



of sediment discharge (e.g., Swift et al., 2005; Delaney et al., 2018b) compared to the one-dimensional version of SUGSET (e.f. Delaney et al., 2019). Furthermore, the results show that the location of bedrock erosion, processes in the till layer, and the timing of melt all play an important role in the quantity of sediment discharge and the peak sediment discharge that is reached.

In the final case, we compared model runs across a parameter space. When we compare the model runs across the space of three parameters,  $D_m$ ,  $B$ , and  $H_0$ , to sediment discharge data from Griesgletscher in the Swiss Alps (Section 3.2). The limited ability of the model we find that the model has a limited ability to capture the large sediment discharge from the first time period and the minimum (2011-2013). The reduced sediment discharge in the second and fourth time periods show that processes not adequately represented in the model, 2013 - 2014 and 2015 - 2016, indicates that the model does not adequately represent the processes that are responsible for the increase measured increases in sediment transport at this time these time periods (Figure 8). Such processes may include activation of new patches of the glacier bed or the relocation of channels (e.g., Zechmann et al., 2020), potentially due to changes to glacier surface topography that variable flow routing following channel shape (Equations 1 and 2) or flotation fraction (Equation 16). Additional processes may also be omitted due to model inputs. For instance, the evolving surface topography, not considered here, may cause alternative flow paths below the glacier (Fischer et al., 2005) and exposes new patches of the glacier bed to sediment transport or the relocation of channels (e.g., Zechmann et al., 2020). Furthermore, glacier sliding remains constant over the model run. In turn, so the results do not explicitly account for seasonal or interannual variability in bedrock erosion (e.g., Herman et al., 2015) (e.g., Herman et al., 2015; Ugelvig et al., 2018); however, temporal variations in bedrock erosion are calculated through changing till thickness (Equation 12 and Figure 9).

Model performance at Griesgletscher depends greatly on sediment grain size, as compared to other parameters such as the initial till condition or bedrock erosion (Figure 8 c, d). Grain size is a strong control in the on sediment discharge in SUGSET\_2D because it modulates how easily sediment is mobilized sediment mobilization in patches of the bed only occasionally accessed by sub-glacial flow during the melt season — after sediment has been largely evacuated from the main channel (Figure 11). This process cannot be fully considered represented in a one-dimensional model, though this processes seems important on this relatively small and shallow alpine glacier. These results show that connectivity between subglacial channels and distal sediment patches is a strong control on sediment discharge from the subglacial system. This is especially so because the main flow paths under the glacier can be evacuated of sediment (Figure 11 c, d). Thus, these flow paths contribute to the catchment's sediment discharge only through the new production of sediment through erosion (Equation 12). However, the dependence on grain size suggests that the connectivity between subglacial channels and distal sediment patches is a strong control on sediment discharge from the subglacial system. While this seems to be an important process on the relatively small and shallow Griesgletscher alpine glacier Delaney et al. (2018a), sediment discharge on other, potentially steeper, glaciers may respond more strongly to processes such as bedrock erosion (Herman et al., 2015). The connectivity between the main channels and distal sources of sediment could be through the transport of small sediments as applied occurs through the fluvial transport capacity of sediments here, but may also occur through other this connectivity may also be influenced through processes

not considered in the model, such as till deformation (e.g., Damsgaard et al., 2020) or sediment sorting (e.g. Bacchi et al., 2014).

500 Lastly, the model demonstrates the complex nature of subglacial sediment transport and the transitions between supply- and transport-limited regimes. Sediment discharge depends not only on hydrology but also on the sediment availability. transport-limited regimes. Equivalent values of water input and sediment transport capacity below the glacier result in simulated sediment discharge discharges that vary over orders of magnitude (Figure 10, a). In turn, using solely the water discharge or sediment transport capacity (e.g. , Equation 8) fails to consider the changes to sediment availability caused by sediment transport, especially when changes to sediment storage can take place over seasons to decades. Finding ways to evaluate these  
505 difficult to measure parameters could be key to improving our understanding of subglacial sediment transport. seasonal to decadal time scales.

## 6 Conclusions

~~We present a~~ A two-dimensional subglacial sediment transport model, SUGSET\_2D, that evolves a till layer in response to subglacial hydrology, changing subglacial hydraulic conditions. The model represents sediment transport in supply- and  
510 transport-limited regimes, and sediment and water are routed across the bed in response to changing hydraulic conditions in two horizontal dimensions. The till layer is supplied with sediment either from bedrock erosion or by existing sediment, represented by the initial condition. Model cases utilize geometries and hydrological forcings from a synthetic and a real alpine glacier. The model captures sediment transport in supply- and transport-limited regimes. Results from both cases point to the need to quantify the spatial distribution of subglacial sediment and water when simulating sediment discharge expelled from  
515 glaciers. Model outputs reproduce many observed subglacial sediment processes. case and Griesgletscher, an alpine glacier in the Swiss Alps.

Despite the model's ability to reproduce observations, it relies on The interdependence of a large number of poorly constrained parameters. For instance, parameters and their interaction with one another, for instance, sliding and erosion (Equations 12 to 15),  
520 in the very least point to our knowledge, only one study has quantified till thickness at a single point below a glacier (Truffer et al., 2000). These observations are limited due to the difficulty of making direct observations at glacier beds. The initial till height,  $H_0$ , in the model, therefore, must be chosen thoughtfully because the system remains impacted by this condition throughout the model run.

This two-dimensional sediment transport model can represent several observed characteristics of subglacial sediment discharge compared to the one-dimensional version. SUGSET\_2D routes water and sediment using the Shreve potential and a spatially  
525 uniform flotation fraction that evolves in time in the real glacier case (e. g., Section 3.2). Future work may consider using a coupled model of channelized and distributed drainage networks (Hewitt, 2013; Werder et al., 2013). Increasing the sophistication of the subglacial hydrology model may better evaluate the locations of high sediment transport capacity. Such models could even be run offline if the operator assumes, as we do, that rates of change in till height are small compared to the evolution in cross-section of the subglacial conduit.

530 ~~Our simulations highlight that increased glacier melt does not necessarily result in commensurate changes to sediment discharge unless new previously inaccessible subglacial sediment patches are accessed by meltwater. Additionally, results demonstrate the role of spatially varying water routing and lateral sediment connectivity in subglacial sediment discharge. Further efforts should constrain the role of changing glacial dynamics on erosion and the complexity of sediment transport in the subglacial system. Furthermore, the model's limited representation of the magnitude of interannual variability in the~~  
535 ~~Griesgletscher simulation, from 2011 to 2017, points to processes not completely represented in this application of the model. This misfit could come from poorly constrained parameters and external factors, such as model inputs that may limit the model's accurate representation of sediment transport. Further modeling and observational studies are needed to better constrain the timescales over which these processes occur in a changing climate.~~ discharge observations. These include interannual variability of glacier velocity and, thus, bedrock erosion, changing glacier topography that routes water to different patches of  
540 the glacier bed over time, and routing of water to the glacier bed.

Additional insights into subglacial erosion and sediment transport processes over decadal timescales can be gained from more sophisticated parameterizations of bedrock erosion and subglacial hydrology. Even so, the foundational processes of the model presented here should be considered when examining subglacial sediment transport processes at seasonal to decadal scales. These processes include: 1) fluvial transport of subglacial sediment across a glacier's bed in two dimensions in supply- and transport-limited regimes, 2) spatially-distributed bedrock erosion or sediment production, and 3) variable water routing in response to changing melt and hydraulic conditions. It is our hope that the model will be applied in the context of field observations to evaluate and isolate subglacial processes controlling sediment discharge from glaciers as they change.

545

*Code availability.* The code library and illustrative examples are available at <https://bitbucket.org/IanDelaney/sugset.jl/src/id-2d>. The running and plotting scripts used in the cases herein are stored at [https://bitbucket.org/IanDelaney/2d\\_runners/src/master/](https://bitbucket.org/IanDelaney/2d_runners/src/master/).

550 *Video supplement.* Videos of a prior model version's application to Griesgletscher are available at <https://bit.ly/3nPvVUI>, demonstrating model behavior. Similar videos of the current model version will be transferred to a permanent location pending acceptance.

*Author contributions.* ID designed the study, developed the model, ran the cases, and lead writing the manuscript. LA assisted with writing the manuscript and provided key advice on designing and troubleshooting the model. FH provided guidance with implementing and designing the model and preparing the manuscript.

555 *Competing interests.* The authors declare no competing interests.

*Acknowledgements.* We thank J. Braun, B. Bovy, F. De Doncker, G. Jouvét, S. N. Lane, G. Prasicek, and M. Werder for fruitful discussions and insightful comments. We are also grateful to Grégoire Mariéthoz and the Scientific Computing and Research Support Unit at Université de Lausanne for providing computing resources. [G. Vance provided comments on the writing.](#) I. Delaney was funded in part by SNF Project No. PZ00P2\_202024. I. Overeem, S. Hergarten, and two anonymous reviewers provided thoughtful and constructive comments that greatly improved this manuscript.

## References

- Alley, R. B., Cuffey, K. M., Evenson, E. B., Strasser, J. C., Lawson, D. E., and Larson, G. J.: How glaciers entrain and transport basal sediment: physical constraints, *Quaternary Science Reviews*, 16, 1017–1038, [https://doi.org/10.1016/S0277-3791\(97\)00034-6](https://doi.org/10.1016/S0277-3791(97)00034-6), 1997.
- Alley, R. B., Lawson, D. E., Larson, G. J., Evenson, E. B., and Baker, G. S.: Stabilizing feedbacks in glacier-bed erosion, *Nature*, 424, 565–758–760, <https://doi.org/10.1038/nature01839>, 2003.
- Andersen, J. L., Egholm, D. L., Knudsen, M. F., Jansen, J. D., and Nielsen, S. B.: The periglacial engine of mountain erosion– Part 1: Rates of frost cracking and frost creep, *Earth Surface Dynamics*, 3, 447–462, <https://doi.org/10.5194/esurf-3-447-2015>, <https://esurf.copernicus.org/articles/3/447/2015/>, 2015.
- Bacchi, V., Recking, A., Eckert, N., Frey, P., Piton, G., and Naaim, M.: The effects of kinetic sorting on sediment mobility on steep slopes, *Earth Surface Processes and Landforms*, 39, 1075–1086, <https://doi.org/10.1002/esp.3564>, 2014.
- Beaud, F., Flowers, G., and Venditti, J. G.: Modeling sediment transport in ice-walled subglacial channels and its implications for esker formation and pro-glacial sediment yields, *Journal of Geophysical Research: Earth Surface*, 123, 1–56, <https://doi.org/10.1029/2018JF004779>, 2018a.
- Beaud, F., Venditti, J., Flowers, G., and Koppes, M.: Excavation of subglacial bedrock channels by seasonal meltwater flow, *Earth Surface Processes and Landforms*, 43, 1960–1972, <https://doi.org/10.1002/esp.4367>, 2018b.
- Bhatia, M. P., Kujawinski, E. B., Das, S. B., Breier, C. F., Henderson, P. B., and Charette, M. A.: Greenland meltwater as a significant and potentially bioavailable source of iron to the ocean, *Nature Geoscience*, 6, 274, 2013.
- Bovy, B., Braun, J., and Demoulin, A.: A new numerical framework for simulating the control of weather and climate on the evolution of soil-mantled hillslopes, *Geomorphology*, 263, 99 – 112, <https://doi.org/https://doi.org/10.1016/j.geomorph.2016.03.016>, 2016.
- 580 Brinkerhoff, D., Truffer, M., and Aschwanden, A.: Sediment transport drives tidewater glacier periodicity, *Nature Communications*, 8, 90, <https://doi.org/10.1038/s41467-017-00095-5>, 2017.
- Brinkerhoff, D. J., Meyer, C. R., Bueler, E., Truffer, M., and Bartholomaus, T. C.: Inversion of a glacier hydrology model, *Annals of Glaciology*, 57, 84–95, 2016.
- Chen, Y., Liu, X., Gulley, J. D., and Mankoff, K. D.: Subglacial Conduit Roughness: Insights From Computational Fluid Dynamics Models, *Geophysical Research Letters*, 45, 11,206–11,218, <https://doi.org/10.1029/2018GL079590>, 2018.
- 585 Church, M. and Ryder, J. M.: Paraglacial sedimentation: a consideration of fluvial processes conditioned by glaciation, *Geological Society of America Bulletin*, 83, 3059–3072, 1972.
- Cook, S., Swift, D., Kirkbride, M., Knight, P., and Waller, R.: The empirical basis for modelling glacial erosion rates, *Nature communications*, 11, 1–7, <https://doi.org/10.1038/s41467-020-14583-8>, 2020.
- 590 Covington, M. D., Gulley, J. D., Trunz, C., Mejia, J., and Gadd, W.: Moulin Volumes Regulate Subglacial Water Pressure on the Greenland Ice Sheet, *Geophysical Research Letters*, 47, e2020GL088 901, <https://doi.org/https://doi.org/10.1029/2020GL088901>, <https://agupubs.onlinelibrary.wiley.com/doi/abs/10.1029/2020GL088901>, 2020.
- Creys, T. T., Clarke, G. K. C., and Church, M.: Evolution of subglacial overdeepenings in response to sediment redistribution and glaciohydraulic supercooling, *Journal of Geophysical Research: Earth Surface*, 118, 423–446, 2013.
- 595 Cuffey, K. M. and Paterson, W. S. B.: *The Physics of Glaciers*, Butterworth-Heinemann, Burlington, MA, USA, Forth edn., 2010.
- Damsgaard, A., Goren, L., and Suckale, J.: Water pressure fluctuations control variability in sediment flux and slip dynamics beneath glaciers and ice streams, *Communications Earth & Environment*, 1, 1–8, <https://doi.org/10.1038/s43247-020-00074-7>, 2020.

- de Fleurian, B., Werder, M. A., Beyer, S., Brinkerhoff, D., Delaney, I., Dow, C., Downs, J., Hoffman, M., Hooke, R., Seguinot, J., and Sommers, A.: SHMIP The Subglacial Hydrology Model Intercomparison Project, *Journal of Glaciology*, 64, 897–916, <https://doi.org/10.1017/jog.2018.78>, 2018.
- 600 Delaney, I. and Adhikari, S.: Increased subglacial sediment discharge during century scale glacier retreat: consideration of ice dynamics, glacial erosion and fluvial sediment transport, *Geophysical Research Letters*, p. e2019GL085672, <https://doi.org/10.1029/2019GL085672>, 2020.
- Delaney, I. and Anderson, L. S.: Debris Cover Limits Subglacial Erosion and Promotes Till Accumulation, *Geophysical Research Letters*, 605 49, e2022GL099049, <https://doi.org/10.1029/2022GL099049>, e2022GL099049 2022GL099049, 2022.
- Delaney, I., Bauder, A., Huss, M., and Weidmann, Y.: Proglacial erosion rates and processes in a glacierized catchment in the Swiss Alps, *Earth Surface Processes and Landforms*, 43, 765–778, <https://doi.org/10.1002/esp.4239>, 2018a.
- Delaney, I., Bauder, A., Werder, M. A., and Farinotti, D.: Regional and annual variability in subglacial sediment transport by water for two glaciers in the Swiss Alps, *Frontiers in Earth Science*, <https://doi.org/10.3389/feart.2018.00175>, 2018b.
- 610 Delaney, I., Werder, M., and Farinotti, D.: A Numerical Model for Fluvial Transport of Subglacial Sediment, *Journal of Geophysical Research: Earth Surface*, 124, 2197–2223, <https://doi.org/10.1029/2019JF005004>, 2019.
- Egholm, D., Nielsen, S., Pedersen, V., and Lesemann, J.-E.: Glacial effects limiting mountain height, *Nature*, 460, 884–887, <https://doi.org/10.1038/nature08263>, 2009.
- Egholm, D. L., Pedersen, V. K., Knudsen, M. F., and Larsen, N. K.: Coupling the flow of ice, water, and sediment in a glacial landscape evolution model, *Geomorphology*, 141, 47–66, 2012.
- 615 Engelund, F. and Hansen, E.: A monograph on sediment transport in alluvial streams, Tech. rep., Technical University of Denmark, Copenhagen, Denmark, 1967.
- Exner, F. M.: Über die Wechselwirkung zwischen Wasser und Geschiebe in flüssen, *Abhandlungen der Akademie der Wissenschaften, Wien*, 134, 165–204, 1920a.
- 620 Exner, F. M.: Zur Physik der Dünen, *Abhandlungen der Akademie der Wissenschaften, Wien*, 129, 929–952, 1920b.
- Felix, D., Albayrak, I., Abgottspon, A., and Boes, R. M.: Suspended sediment measurements and calculation of the particle load at HPP Fieschertal, *IOP Conference Series: Earth and Environmental Science*, 49, 122007, <https://doi.org/10.1088/1755-1315/49/12/122007>, <http://stacks.iop.org/1755-1315/49/i=12/a=122007>, 2016.
- Fischer, U. H., Braun, A., Bauder, A., and Flowers, G. E.: Changes in geometry and subglacial drainage derived from digital elevation models: Unteraargletscher, Switzerland, 1927–97, *Annals of Glaciology*, 40, 20–24, <https://doi.org/10.3189/172756405781813528>, 2005.
- 625 Gimbert, F., Tsai, V. C., Amundson, J. M., Bartholomäus, T. C., and Walter, J. I.: Subseasonal changes observed in subglacial channel pressure, size, and sediment transport, *Geophysical Research Letters*, 43, 3786–3794, 2016.
- Hairer, E., Nørsett, S. P., and Wanner, G.: Solving ordinary differential equations I: nonstiff problems, vol. 1, Springer Science & Business, <http://link.springer.com/book/10.1007/978-3-540-78862-1>, 1992.
- 630 Hallet, B.: A theoretical model of glacial abrasion, *Journal of Glaciology*, 23, 39–50, 1979.
- Hallet, B., Hunter, L., and Bogen, J.: Rates of erosion and sediment evacuation by glaciers: A review of field data and their implications, *Global and Planetary Change*, 12, 213–235, [https://doi.org/10.1016/0921-8181\(95\)00021-6](https://doi.org/10.1016/0921-8181(95)00021-6), 1996.
- Harbor, J., Hallet, B., and Raymond, C.: A numerical model of landform development by glacial erosion, *Nature*, 333, 347, 1988.

- Hawkings, J., Wadham, J., Tranter, M., Raiswell, R., Benning, L., Statham, P., Tedstone, A., Nienow, P., Lee, K., and Telling, J.: Ice sheets as a significant source of highly reactive nanoparticulate iron to the oceans, *Nature communications*, 5, 1–8, <https://doi.org/10.1038/ncomms4929>, 2014.
- Herman, F., Beaud, F., Champagnac, J., Lemieux, J. M., and Sternai, P.: Glacial hydrology and erosion patterns: a mechanism for carving glacial valleys, *Earth and Planetary Science Letters*, 310, 498–508, <https://doi.org/10.1016/j.epsl.2011.08.022>, 2011.
- Herman, F., Beysac, O., Brughelli, M., Lane, S. N., Leprince, S., Adatte, T., Lin, J. Y. Y., Avouac, J. P., and Cox, S. C.: Erosion by an alpine glacier, *Science*, 350, 193–195, <https://doi.org/10.1126/science.aab2386>, 2015.
- Herman, F., Braun, J., Deal, E., and Prasicek, G.: The Response Time of Glacial Erosion, *Journal of Geophysical Research: Earth Surface*, 123, 801–817, <https://doi.org/10.1002/2017JF004586>, <https://agupubs.onlinelibrary.wiley.com/doi/abs/10.1002/2017JF004586>, 2018.
- Herman, F., De Doncker, F., Delaney, I., Prasicek, G., and Koppes, M.: The impact of glaciers on mountain erosion, *Nature Reviews Earth & Environment*, 2, 422–435, <https://doi.org/10.1038/s43017-021-00165-9>, 2021.
- Hewitt, I. and Creyts, T.: A model for the formation of eskers, *Geophysical Research Letters*, 46, 6673–6680, <https://doi.org/10.1029/2019GL082304>, 2019.
- Hewitt, I. J.: Seasonal changes in ice sheet motion due to melt water lubrication, *Earth Planetary Science Letters*, 371–372, 16 – 25, <https://doi.org/10.1016/j.epsl.2013.04.022>, 2013.
- Hooke, R. L., Laumann, T., and Kohler, J.: Subglacial Water Pressures and the Shape of Subglacial Conduits, *Journal of Glaciology*, 36, 67–71, <https://doi.org/10.3189/S0022143000005566>, 1990.
- Humphrey, N. and Raymond, C.: Hydrology, erosion and sediment production in a surging glacier: Variegated Glacier, Alaska, 1982–83, *Journal of Glaciology*, 40, 539–552, 1994.
- Iken, A. and Bindshadler, R. A.: Combined measurements of subglacial water pressure and surface velocity of Findelengletscher, Switzerland: conclusions about drainage system and sliding mechanism, *Journal of Glaciology*, 32, 101–119, 1986.
- Iverson, N. R.: Laboratory simulations of glacial abrasion: comparison with theory, *Journal of Glaciology*, 36, 304–314, <https://doi.org/10.3189/002214390793701264>, 1990.
- Iverson, N. R.: A theory of glacial quarrying for landscape evolution models, *Geology*, 40, 679–682, <https://doi.org/10.1130/G33079.1>, 2012.
- Kasmalkar, I., Mantelli, E., and Suckale, J.: Spatial heterogeneity in subglacial drainage driven by till erosion, *Proceedings of the Royal Society A: Mathematical, Physical and Engineering Sciences*, 475, 20190259, <https://doi.org/10.1098/rspa.2019.0259>, 2019.
- Koppes, M., Hallet, B., Rignot, E., Mouginot, J., Wellner, J. S., and Boldt, K.: Observed latitudinal variations in erosion as a function of glacier dynamics, *Nature*, 526, 100–103, 2015.
- Lane, S. N., Bakker, M., Gabbud, C., Micheletti, N., and Saugy, J.: Sediment export, transient landscape response and catchment-scale connectivity following rapid climate warming and alpine glacier recession, *Geomorphology*, 277, 210 – 227, <https://doi.org/10.1016/j.geomorph.2016.02.015>, 2017.
- Li, D., Lu, X., Overeem, I., Walling, D. E., Syvitski, J., Kettner, A. J., Bookhagen, B., Zhou, Y., and Zhang, T.: Exceptional increases in fluvial sediment fluxes in a warmer and wetter High Mountain Asia, *Science*, 374, 599–603, <https://doi.org/10.1126/science.abi9649>, 2021.
- Li, D., Lu, X., Walling, D., Zhang, T., Steiner, J., Wasson, R., Harrison, S., Nepal, S., Nie, Y., Immerzeel, W., et al.: High Mountain Asia hydropower systems threatened by climate-driven landscape instability, *Nature Geoscience*, 15, 520–530, 2022.
- Mao, L., Dell’Agnese, A., Huincahe, C., Penna, D., Engel, M., Niedrist, G., and Comiti, F.: Bedload hysteresis in a glacier-fed mountain river, *Earth Surface Processes and Landforms*, 39, 964–976, <https://doi.org/10.1002/esp.3563>, 2014.

- Meyer-Peter, E. and Müller, R.: Formulas for bedload transport, in: Hydraulic Engineering Reports, International Association for Hydro-Environment Engineering and Research, 1948.
- 675 Milner, A., Khamis, K., Battin, T., Brittain, J., Barr and, N., Füreder, L., Cauvy-Fraunié, S., Gíslason, G., Jacobsen, D., Hannah, D., et al.: Glacier shrinkage driving global changes in downstream systems, *Proceedings of the National Academy of Sciences*, 114, 9770–9778, 2017.
- Nanni, U., Gimbert, F., Vincent, C., Gräff, D., Walter, F., Piard, L., and Moreau, L.: Quantification of seasonal and diurnal dynamics of subglacial channels using seismic observations on an Alpine glacier, *The Cryosphere*, 14, 1475–1496, <https://doi.org/10.5194/tc-14-1475-2020>, 2020.
- 680 Ng, F. S. L.: Canals under sediment-based ice sheets, *Annals of Glaciology*, 30, 146–152, 2000.
- Paola, C. and Voller, V. R.: A generalized Exner equation for sediment mass balance, *Journal of Geophysical Research: Earth Surface*, 110, <https://doi.org/10.1029/2004JF000274>, <https://agupubs.onlinelibrary.wiley.com/doi/abs/10.1029/2004JF000274>, 2005.
- Perolo, P., Bakker, M., Gabbud, C., Moradi, G., Rennie, C., and Lane, S. N.: Subglacial sediment production and snout marginal ice uplift during the late ablation season of a temperate valley glacier, *Earth Surface Processes and Landforms*, 0, 1–68, 685 <https://doi.org/10.1002/esp.4562>, 2018.
- Pohle, A., Werder, M. A., Gräff, D., and Farinotti, D.: Characterising englacial R-channels using artificial moulins, *Journal of Glaciology*, p. 1–12, <https://doi.org/10.1017/jog.2022.4>, 2022.
- Prasicek, G., Herman, F., Robl, J., and Braun, J.: Glacial Steady State Topography Controlled by the Coupled Influence of Tectonics and Climate, *Journal of Geophysical Research: Earth Surface*, 123, 1344–1362, <https://doi.org/https://doi.org/10.1029/2017JF004559>, 2018.
- 690 Prasicek, G., Hergarten, S., Deal, E., Herman, F., and Robl, J.: A glacial buzzsaw effect generated by efficient erosion of temperate glaciers in a steady state model, *Earth and Planetary Science Letters*, 543, 116 350, <https://doi.org/10.1016/j.epsl.2020.116350>, 2020.
- Quinn, P., Beven, K., Chevallier, P., and Planchon, O.: The prediction of hillslope flow paths for distributed hydrological modelling using digital terrain models, *Hydrological processes*, 5, 59–79, 1991.
- Rackauckas, C. and Nie, Q.: DifferentialEquations.jl—A Performant and Feature-Rich Ecosystem for Solving Differential Equations in Julia, 695 *Journal of Open Research Software*, 5, 15, <https://doi.org/10.5334/jors.151>, 2017.
- Radhakrishnan, K. and Hindmarsh, A. C.: Description and use of LSODE, the Livermore solver for ordinary differential equations, Reference Publication 1327, NASA, 1993.
- Riihimäki, C. A., MacGregor, K. R., Anderson, R. ., Anderson, S. P., and Loso, M. G.: Sediment evacuation and glacial erosion rates at a small alpine glacier, *Journal of Geophysical Research: Earth Surface (2003–2012)*, 110, <https://doi.org/10.1029/2004JF000189>, 2005.
- 700 Röthlisberger, H.: Water pressure in intra- and subglacial channels, *Journal of Glaciology*, 11, 177–203, 1972.
- Seguinot, J. and Delaney, I.: Last-glacial-cycle glacier erosion potential in the Alps, *Earth Surface Dynamics*, 9, 923–935, <https://doi.org/10.5194/esurf-9-923-2021>, 2021.
- Shields, A.: Anwendung der Aehnlichkeitsmechanik und der Turbulenzforschung auf die Geschiebebewegung, PhD Thesis Technical University Berlin, 1936.
- 705 Shreve, R. L.: Movement of water in glaciers, *Journal of Glaciology*, 11, 205–214, 1972.
- Swift, D. A., Nienow, P. W., and Hoey, T. B.: Basal sediment evacuation by subglacial meltwater: suspended sediment transport from Haut Glacier d’Arolla, Switzerland, *Earth Surface Processes and Landforms*, 30, 867–883, <https://doi.org/10.1002/esp.1197>, 2005.
- Thapa, B., Shrestha, R., Dhakal, P., and Thapa, B. S.: Problems of Nepalese hydropower projects due to suspended sediments, *Aquatic Ecosystem Health & Management*, 8, 251–257, <https://doi.org/10.1080/14634980500218241>, 2005.



- 710 Truffer, M., Harrison, W. D., and Echelmeyer, K. A.: Glacier motion dominated by processes deep in underlying till, *Journal of Glaciology*, 46, 213–221, 2000.
- Ugelvig, S. V., Egholm, D. L., Anderson, R. S., and Iverson, N. R.: Glacial Erosion Driven by Variations in Meltwater Drainage, *Journal of Geophysical Research: Earth Surface*, 123, <https://doi.org/10.1029/2018JF004680>, 2018.
- 715 Wadham, J., Hawkings, J., Tarasov, L., Gregoire, L., Spencer, R., Gutjahr, M., Ridgwell, A., and Kohfeld, K.: Ice sheets matter for the global carbon cycle, *Nature communications*, 10, 1–17, <https://doi.org/10.1038/s41467-019-11394-4>, 2019.
- Walder, J. S. and Fowler, A.: Channelized subglacial drainage over a deformable bed, *Journal of Glaciology*, 40, 3–15, <https://doi.org/10.3189/S0022143000003750>, 1994.
- Weertman, J.: On the sliding of glaciers, *Journal of Glaciology*, 3, 33–38, 1957.
- 720 Werder, M. A., Hewitt, I. J., Schoof, C. G., and Flowers, G. E.: Modeling channelized and distributed subglacial drainage in two dimensions, *Journal of Geophysical Research: Earth Surface*, 118, 2140–2158, <https://doi.org/10.1002/jgrf.20146>, 2013.
- Willis, I. C., Richards, K. S., and Sharp, M. J.: Links between proglacial stream suspended sediment dynamics, glacier hydrology and glacier motion at Middalsbreen, Norway, *Hydrological Processes*, 10, 629–648, 1996.
- Zechmann, J., Truffer, M., Motyka, R., Amundson, J., and Larsen, C.: Sediment redistribution beneath the terminus of an advancing glacier, Taku Glacier (T'aakú Kwáan Sí't'i), Alaska, *Journal of Glaciology*, p. 1–15, <https://doi.org/10.1017/jog.2020.101>, 2020.

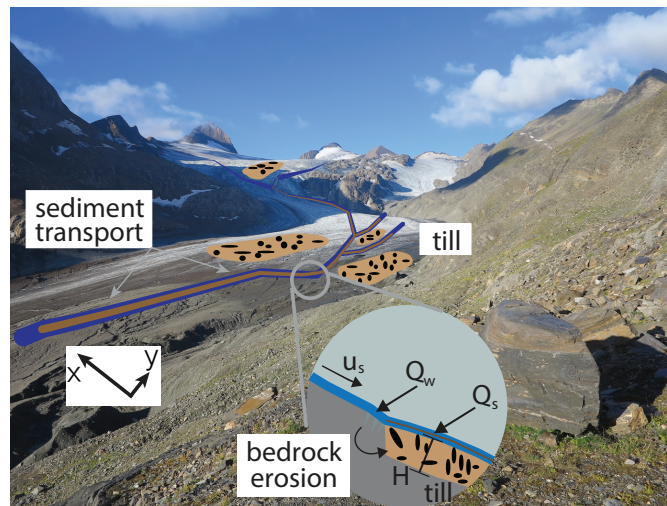


**Figure 1.** Cartoon of erosional and sediment transport processes considered in model overlaid-overlain on an image of Griesgletscher in 2016. Bedrock erosion scales with sliding speed ( $u_s$ ) and adds material to the till layer with thickness ( $H$ ), while water ( $Q_w$ ) transports sediment ( $Q_s$ ) fluvially, if sediment persists in that location of the glacier bed and fluvial transport-conditions are sufficient for transport. [Photo credit I. Delaney.](#)

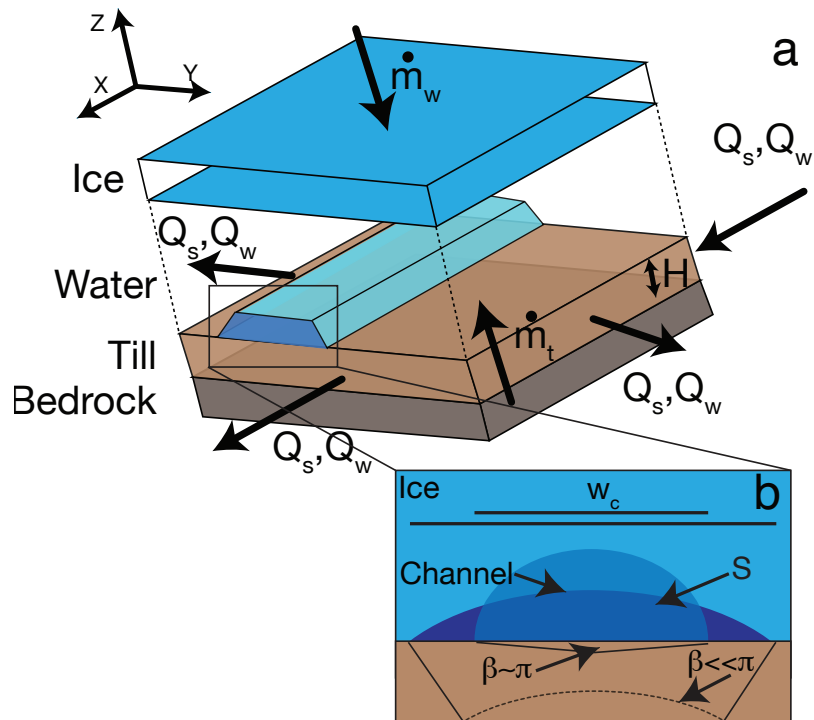


**Figure 2.** Illustration of [terms in Equation 5 model cell \(a\)](#), detailing the layers of bedrock, till, water, and ice. Characteristics of the subglacial channel are [also noted as a polygon](#) but shown in [one-dimension one dimension](#) for clarity [in \(b\)](#) with Hooke angle parameterization with [two different channel shapes for different values of  \$\beta\$](#) , [Equations 2, 9 and 10](#).

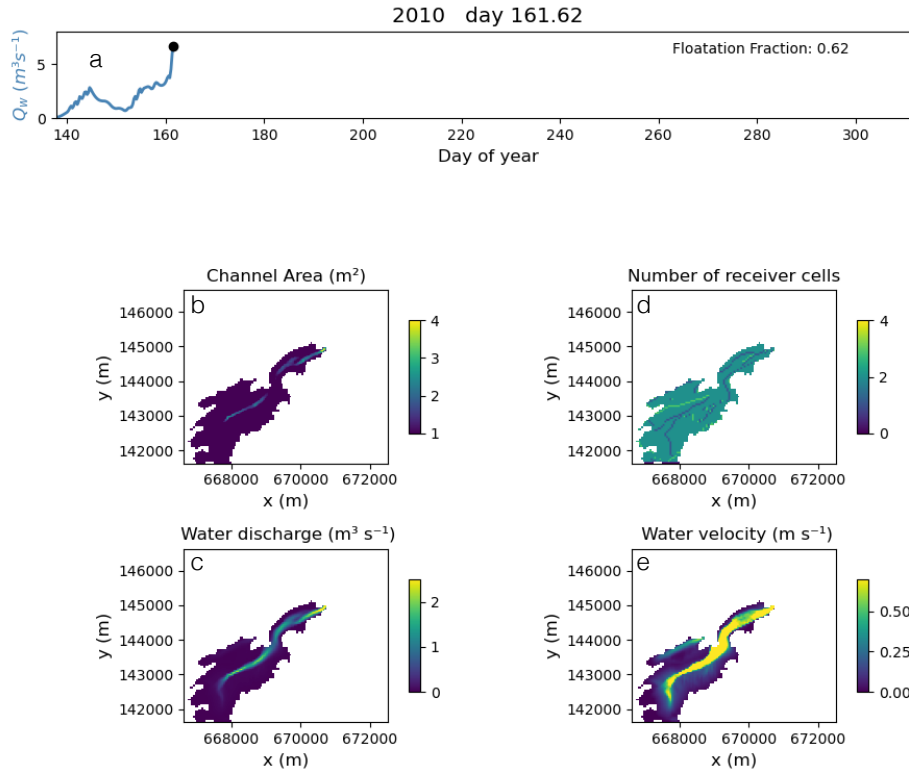


**Figure 3.** Example of model parameters and variables for the ~~snapshot~~ snapshot of the Griesgletscher case Section 3.2. ~~Water discharge from the catchment and glacier floatation fraction~~ (a) ~~Glacier floatation fraction.~~ (b) Channel cross-sectional area  $S$  with (bc) with distributed water discharge, (ed) ; the number of receivers cells,  $r_t$  for a given cell, (de) ; and the water velocity (e). ~~Conditions b-e evolve with different hydrological conditions (e.g. a) over the glacier run.~~

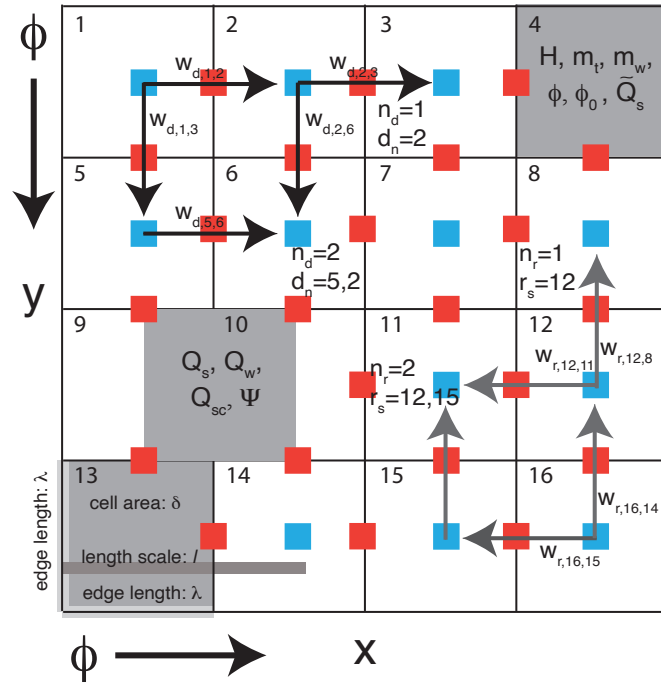


**Figure 4.** Model output from alpine topography Routing scheme on the grid. Solid lines represent cell boundaries, blue squares are cell centers, and forcing over a 30-year run with diurnal and seasonal variations in melt input red squares are cell edges. Grey box represents time period  $\phi$ , the hydraulic potential, decreases in the direction of increasing glacier melt. a) Seasonally varying arrows so that water discharge and sediment generally flow left to right and top to bottom. Edge length ( $Q_w \lambda$ ) increases from year 10 to 20, while till height and cell area ( $H\delta$ ) decreases are shown. b) Annual sediment discharge Cell numbers refer to identification in the stack (green  $s_t$ ) increases over with increasing melt. Select cells denote the weight of donors  $w_{d,i,j}$ , with highest sediment discharge occurring in year 19 number of donors  $n_d$ , when glacier melt is greatest donor cells  $d_n$ , number of receivers  $n_r$ , and receiver cells  $r_s$ . One Variables and their respective locations on the new climate stabilizes, annual sediment discharge stabilizes at a higher level than before grid are shown. Some red and blue squares have been removed in some cells for clarity.

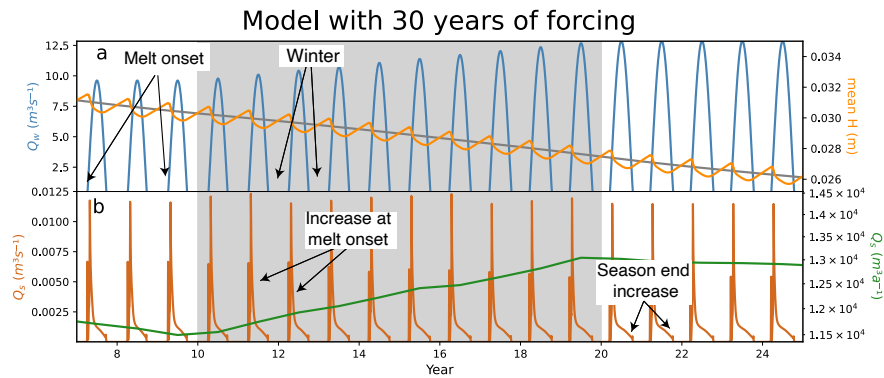


**Figure 5.** Model output from a synthetic alpine topography and forcing over a 30-year run with diurnal and seasonal variations in melt input as daily mean values. The grey box represents a time period of increasing glacier melt. (a) Daily averaged seasonally varying water discharge ( $Q_w$ ) increases from year 10 to 20, while till height ( $H$ ) decreases throughout the model run, with seasonal increases in the absence of glacier melt. (b) Daily averaged sediment discharge in brown shows strong seasonal variability. Annual sediment discharge (green) increases with increasing melt, with the highest sediment discharge occurring in year 19 when glacier melt is greatest. During stable climate temperatures before and after the increase in temperature, annual sediment discharge generally decreases. However, following the melt,  $Q_s$  stabilizes at a higher level due to in the increased area over which sediment is transported.

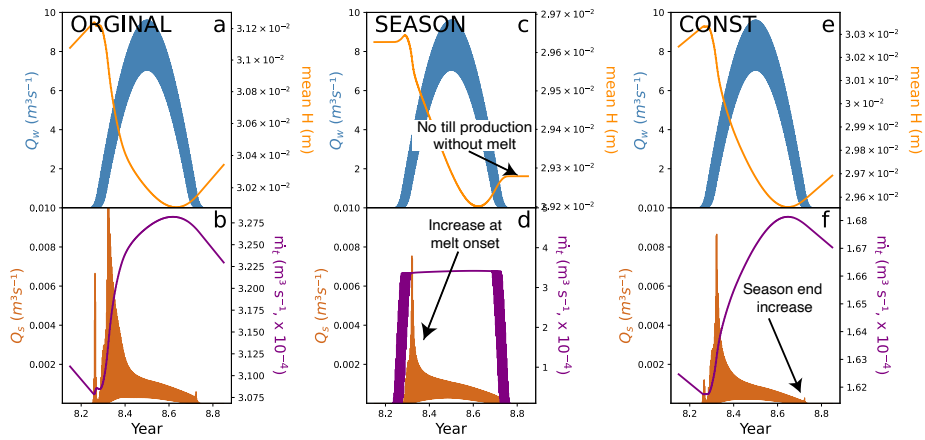


**Figure 6.** Annual response to different till production patterns across the [synthetic glacier case studies](#). (a,b) Conventional model setup, where sediment is produced year-round, *ORIGINAL*. (c,d) Equivalent setup to [the previous](#), except sediment is [only](#)-produced [only](#) in summer months –when water is present at the glacier bed, *SEASON*. Note that till height remains constant [on the edges of the plot](#) over the winter months. (e,f) Steady erosion of  $\pm 2 \text{ mm a}^{-1}$  across the [synthetic glacier](#), with no spatial or temporal variability in sediment production, *CONST*. [Data are plotted at a 6 hr interval so that daily maximums and minimums are visible.](#)

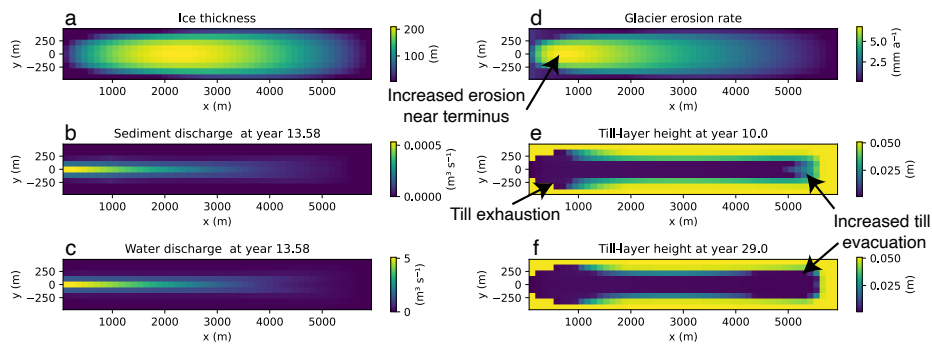


**Figure 7.** Spatial view of ~~subglacial sediment transport-synthetic case~~ (Section 3.1). Spatially distributed (a) ~~ice thickness ( $h$ )~~, ~~water-~~(b) ~~sediment~~ discharge ( $Q_s$ ), (c) ~~water~~ discharge ( $Q_w$ ), ~~till-layer~~(d) ~~glacier~~ erosion rate ( $\dot{e}$ ), (e) ~~till-layer~~ height ( $H$ ) at year 10 prior to ~~increased melt-warming and~~ (bf) ~~and after increased melt~~ ~~till-layer~~ height ( $\delta H$ ) at year 29 near end of model run. Spatial differences in the distribution of water and sediment discharge in plots ~~ae~~) and ~~ef~~) result from the depletion of subglacial till beneath the glacier. We have included an animation of this figure in the video supplement.



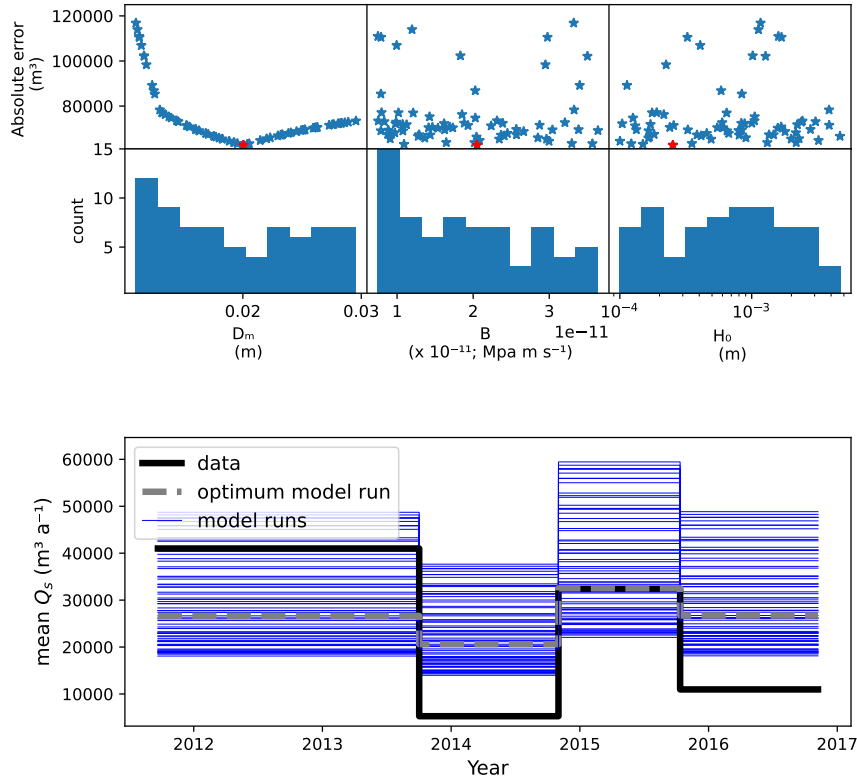


**Figure 8.** Results of the parameter search (a, b, c), the frequency of parameter values that produced a rank correlation of 1 (d, e, f) and **the best fit average sediment flux from** model run amongst the parameter combinations **over the time periods** (g) **in the Griesgletscher case**. Red stars represent **the optimum parameter combination with an absolute error of roughly 62,600 m $^3$** . Blue lines represent all model outputs, while **the** gray line represents the optimum parameter combination.

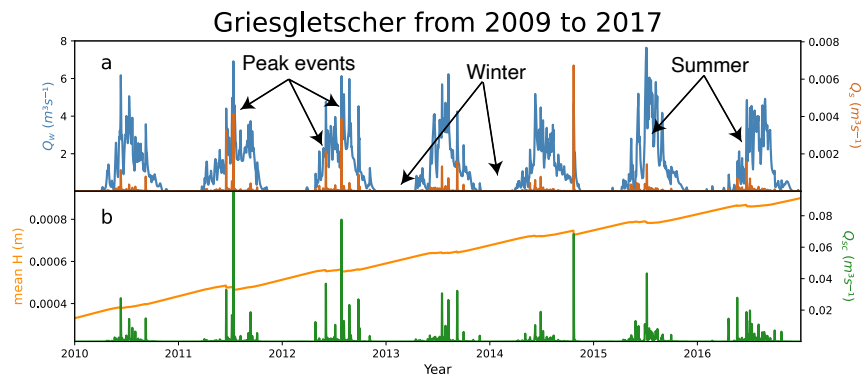


**Figure 9.** Water-Time series of model output from optimum parameter combinations. (a) Daily averaged water discharge, an input modeled for Griesgletscher, Switzerland, in (Delaney et al., 2018b), and sediment discharge, the output of the model, from Griesgletscher beginning in 2010. (ab) Sediment-Daily averaged sediment transport capacity and average till height (b) is below. Note that sediment discharge capacity is roughly one order of magnitude larger than sediment transport discharge. Additionally, the increase-increasing trend in till height,  $H$ , through this model run shows that sediment is produced at a greater rate than it is transported from the glacier bed.

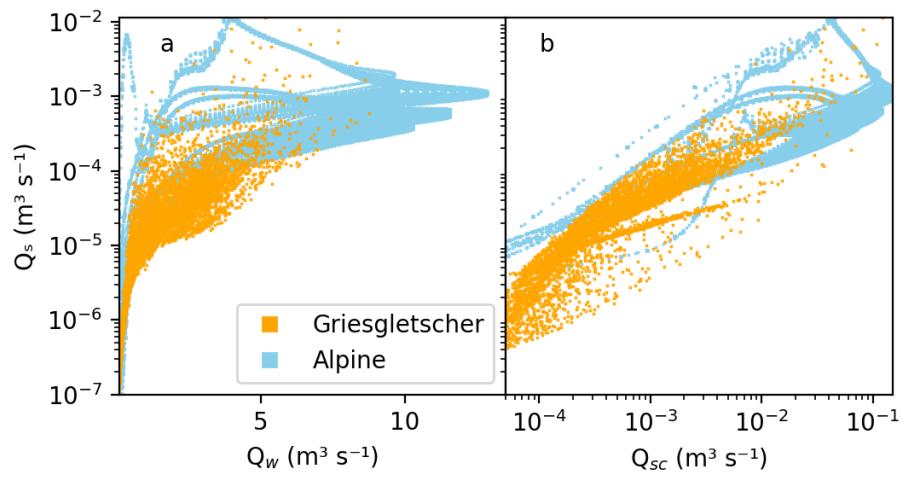


**Figure 10.** Model outputs of sediment discharge from the glacier compared to water discharge (a) and sediment transport capacity (b).

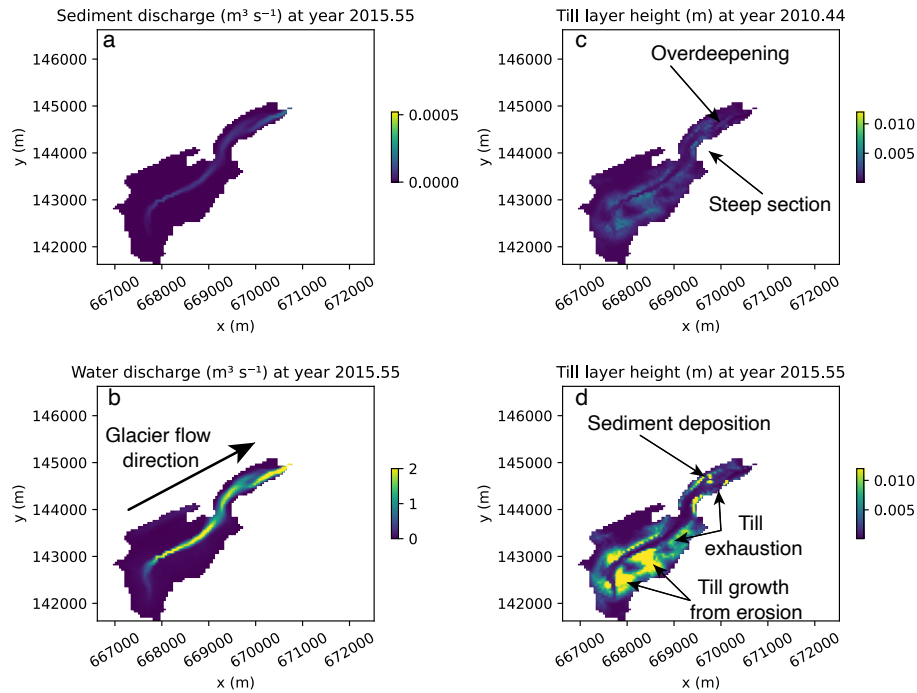


**Figure 11.** Spatial view of characteristics from the Griesgletscher model run ~~-(see Figure 1 shows images of this glacier).~~ (a) Subglacial sediment transport ~~(is concentrated in a narrow part of the bed, (b) and water discharge (e) are is, as well~~ highly variable across the bed. Till layer height changes substantially from the beginning of the model run (c) to ~~after the end of the~~ model run (d). We identify the overdeepening near the glacier terminus as well as ~~as a steep section connected connecting~~ the upper and lower glacier. Over this time, till exhaustion in regions of high water flow is visible, while ~~other~~ regions of ~~the glacier bed experiencing~~ sediment deposition and till growth from glacier erosion can be identified. We have included an animation of this figure in the video supplement.



**Table 1.** Model variables

Name	Symbol	Units
Horizontal (x,y) <del>vertical</del> and time coordinates	<del><math>x, y, z, t</math></del> $x, y, t$	m, m, s
Surface and bed elevation	$z_s, z_b$	m, m, m
<u>Width of glacier bed region</u>	$w$	m
Glacier surface slope	$\alpha$	-
<u>Ice thickness</u>	$h$	m
Channel hydraulic diameter	$D_h$	m
Width of channel floor	$w_c$	m
Channel cross-sectional area	$S$	m <sup>2</sup>
Water discharge (instantaneous)	$Q_w$	m <sup>3</sup> s <sup>-1</sup>
Water source term	$\dot{m}_w$	m s <sup>-1</sup>
Representative water discharge	$Q_w^*$	m <sup>3</sup> s <sup>-1</sup>
Hydraulic potential	$\phi$	Pa
Gradient of $\phi$	$\Psi$	Pa m <sup>-1</sup>
Representative gradient of $\phi$	$\Psi^*$	Pa m <sup>-1</sup>
Flotation fraction	$f_f$	-
Water velocity	$v$	m s <sup>-1</sup>
Water shear-stress	$\tau$	Pa
Till source term	$\dot{m}_t$	m s <sup>-1</sup>
Sediment discharge	$Q_s$	m <sup>3</sup> s <sup>-1</sup>
Sediment discharge capacity	$Q_{sc}$	m <sup>3</sup> s <sup>-1</sup>
<u>Sediment mobilization</u>	$\tilde{Q}_s$	m <sup>2</sup> s <sup>-1</sup>
Glacier sliding velocity	$u_b$	m s <sup>-1</sup>
Basal shear stress	$\tau_b$	MPa
Erosion rate	$\dot{e}$	m s <sup>-1</sup>
<u>Temperature</u>	$T$	C
Till layer height	$H$	m
Mass-balance rate at terminus	$\dot{b}^0$	m s <sup>-1</sup>
<u>Temperature offset</u>	$\Delta T$	C

**Table 2.** Physical model parameters and constants

Name	Symbol	Value	Units
Darcy-Weisbach friction factor	$f_r$	Alpine: 15; Gries: 5	-
Hooke angle of channel	$\beta$	30	°
Source percentile	$s_p$	Alpine: 0.75; Gries: .2	-
Source average time	$s_a$	Alpine: 2.5; Gries: 4.5	d
Sediment-uptake $e$ -folding length	$l$	100	m
Sediment grain mean diameter	$D_m$	Alpine: 0.01; Gries: 0.02	m
Initial till height	$H_0$	Alpine:0.05; Gries: 0.0025	m
Till height limit	$H_{lim}$	0.10	m
Till height erosion limit	$H_g H_{max}$	0.05	m
Gravitational constant	$g$	9.81	$\text{m s}^{-2}$
Density of water	$\rho_w$	1000	$\text{kg m}^{-3}$
Density of ice	$\rho_i$	900	$\text{kg m}^{-3}$
Density of bedrock	$\rho_b$	2650	$\text{kg m}^{-3}$
Bulk density of sediment	$\rho_s$	1500	$\text{kg m}^{-3}$
Erosional exponent	$l_{er}$	2.02	-
Erosional constant	$k_g$	$2.7 \times 10^{-7}$	$\text{m}^{1-l_{er}} \text{s}^{l_{er}-1}$
Seconds per year	$s_{year}$	$3.1536 \times 10^7$	s
Seconds per day	$s_{day}$	86,400	s
<del>Glen's <math>n</math></del> Annual temp. amplitude	<del><math>n A_g</math></del>	<del>3-16</del>	-C
Ice flow rate Diurnal temp. amplitude	$A_d$	2	C
Temperature lapse rate	$\frac{dT}{dz}$	-0.0075	$\text{C m}^{-1}$
Melt factor	$A M_f$	<del><math>2.4 \times 10^{-24}</math></del> 0.01	$\text{m C}^{-1} \text{d}^{-1}$
Mass-balance gradient	$\gamma$	0.00625	$\text{a}^{-1}$
Basal melt rate	$\dot{m}_b$	$7.3 \times 10^{-11}$	$\text{m s}^{-1}$
Sliding rate factor	$B$	Alpine: $3.2 \times 10^{-12}$ ; Gries: $2.05 \times 10^{-11}$	$\text{MPa m s}^{-1}$
Sliding exponent	$m$	1	-

**Table 3.** Numerical model parameters

Name	Symbol	Value	Units
Solver tolerance (relative)	reltol	$10 \times 10^{-8}$	-
Solver tolerance (absolute)	abstol	$10 \times 10^{-8}$	m
Maximum timestep	dtmax	21600 (6)	s (hr)
Minimum timestep	dtmin	1	s
Edge length	$\lambda$		m
Cell area	$\delta$		m <sup>2</sup>
Sediment connectivity factor	$\Delta\sigma$	<del><math>10^3</math></del> $10^{-3}$	m <sup>-1</sup>
Minimum <del>cross-section</del> hydraulic diameter	<del><math>S_{min}</math></del> $Dh_{min}$	<del>0.5</del> $0.3$	m
Number of cells	$n_n$	-	-
Stack	$s_t$	$\vec{n}_n$	-
Receivers	$r_s$	$4 \times n_n$	-
Number of receivers per cell	$n_r$	$\vec{n}_n$	-
Donors	$d_n$	$4 \times n_n$	-
Number of donors per cell	$n_d$	$\vec{n}_n$	-
Weight of each receiver	$w_r$	$4 \times n_n$	-
<u>Weight of each donor</u>	<u><math>w_d</math></u>	$4 \times n_n$	-